

# 1 Probing Fluorinated Motifs onto Dual AChE-MAO B Inhibitors: 2 Rational Design, Synthesis, Biological Evaluation, and Early-ADME 3 Studies

4 Mariagrazia Rullo, Marco Cipolloni, Marco Catto, Carolina Colliva, Daniela Valeria Miniero,  
5 Tiziana Latronico, Modesto de Candia, Tiziana Benicchi, Anna Linusson, Nicola Giacchè,  
6 Cosimo Damiano Altomare, and Leonardo Pisani\*



Cite This: <https://doi.org/10.1021/acs.jmedchem.1c01784>



Read Online

ACCESS |



Metrics & More

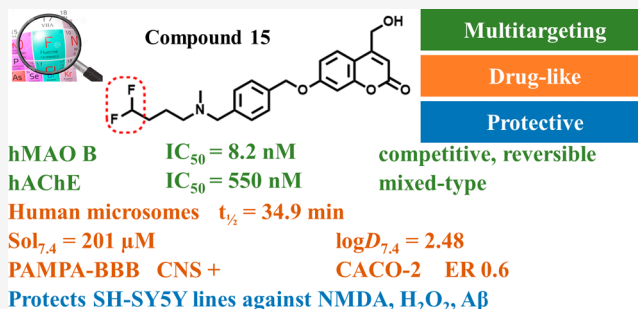


Article Recommendations



Supporting Information

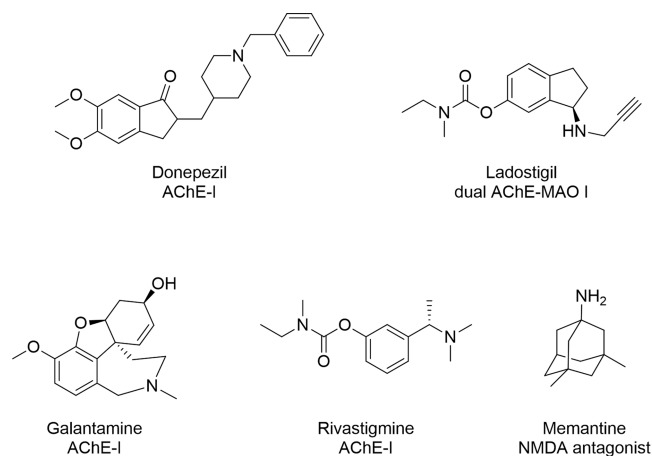
7 **ABSTRACT:** Bioisosteric H/F or CH<sub>2</sub>OH/CF<sub>2</sub>H replacement  
8 was introduced in coumarin derivatives previously characterized as  
9 dual AChE-MAO B inhibitors to probe the effects on both  
10 inhibitory potency and drug-likeness. Along with in vitro screening,  
11 we investigated early-ADME parameters related to solubility and  
12 lipophilicity (Sol<sub>7,4</sub>, CHI<sub>7,4</sub>, log D<sub>7,4</sub>), oral bioavailability and  
13 central nervous system (CNS) penetration (PAMPA-HDM and  
14 PAMPA-blood–brain barrier (BBB) assays, Caco-2 bidirectional  
15 transport study), and metabolic liability (half-lives and clearance in  
16 microsomes, inhibition of CYP3A4). Both specific and nonspecific  
17 tissue toxicities were determined in SH-SY5Y and HepG2 lines,  
18 respectively. Compound **15** bearing a –CF<sub>2</sub>H motif emerged as a  
19 water-soluble, orally bioavailable CNS-permeant potent inhibitor of both human AChE (IC<sub>50</sub> = 550 nM) and MAO B (IC<sub>50</sub> = 8.2  
20 nM, B/A selectivity > 1200). Moreover, **15** behaved as a safe and metabolically stable neuroprotective agent, devoid of cytochrome  
21 liability.



## 22 ■ INTRODUCTION

23 As life expectancy is getting higher, the global impact of age-  
24 related diseases increases its burden on the socioeconomic cost  
25 for caregiving.<sup>1</sup> More than 50 million people live with dementia  
26 worldwide, mostly associated with Alzheimer's disease (AD).<sup>2,3</sup>  
27 Unfortunately, these figures are predicted to more than triple by  
28 the next two decades, unless real effective treatments become  
29 available to clinicians. Huge efforts devoted to the compre-  
30 hension of AD<sup>4</sup> mapped a multifactorial landscape enrolling  
31 much more than 100 mechanisms continuously enriched within  
32 the Aetionomy project.<sup>5</sup> Despite great improvement scored in  
33 disease knowledge and understanding, effective therapies are  
34 still elusive also as the consequence of lacking a unique  
35 druggable etiological event.<sup>6</sup> After memantine (Chart 1), a  
36 glutamate NMDA-receptor blocker able to improve language  
37 and memory skills approved by EMA (2002) and FDA (2003),  
38 no more drug has joined the toolbox for AD therapy with the  
39 exception of an amyloid-directed monoclonal antibody,  
40 aducanumab. Therefore, the cornerstone of Alzheimer's treat-  
41 ment is still occupied by three acetylcholinesterase (AChE)  
42 inhibitors (Chart 1; rivastigmine, galantamine, donepezil),<sup>7</sup> able  
43 to control symptoms in the early stage of the disease without  
44 preventing nor delaying neurotoxic cascade ultimately fatal.<sup>8</sup>  
45 The high failure rate associated with adverse outcomes for most

Chart 1. Small Molecules Approved by FDA or under Clinical Trials for AD Treatment



Received: October 18, 2021

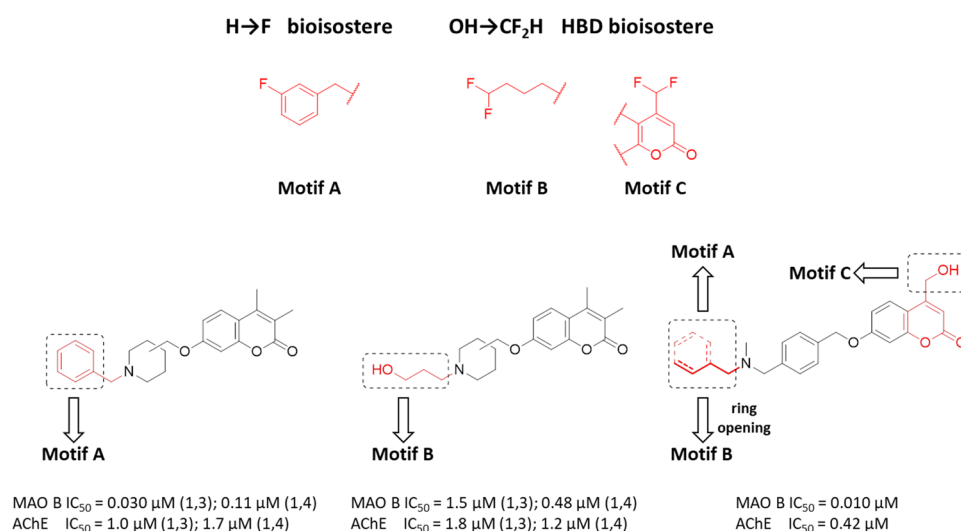


**Figure 1.** Rational design of fluorinated (bio)isosteres. Biological data are referred to human MAO B and electric eel AChE, as already reported in the literature.<sup>18,33,34</sup>

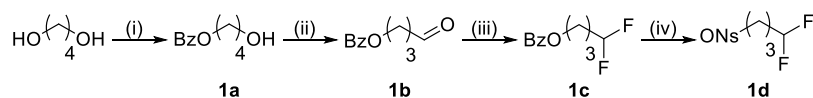
46 phase II/III clinical trials<sup>9</sup> discouraged massive investment in  
47 the field, draining resources progressively away from AD  
48 research. At present, the drug development pipeline counts  
49 more than 100 different agents showing diverse mechanisms of  
50 action, always more frequently distancing amyloid cascade.<sup>10</sup>

51 The urgent need for disease-modifying therapies encouraged  
52 researchers to devise alternatives to single-targeting molecules  
53 along with cutting-edge multitarget strategies.<sup>11</sup> Already  
54 successfully applied to the treatment of cancer and cardiovas-  
55 cular diseases, polypharmacology protocols rooted in drug  
56 cocktails or fixed-dose combinations of active ingredients  
57 provide the control of symptoms and halt/delay the progression  
58 of such complex multifactorial diseases. As a particular case of  
59 polypharmacology, according to definitions, multitarget direc-  
60 ted ligands (MTDLs) or designed multiple ligands (DMLs)  
61 stand for single-molecular entities intentionally designed to  
62 modulate simultaneously two or more targets relevant for  
63 disease pathogenesis. The combination of biochemical mech-  
64 anisms might raise the hope for a real disease-modifying effect  
65 thanks to synergic or additive activities. To this extent, the right  
66 choice of networked biological targets is a major concern. More  
67 recently, different combinations of targets (dual 5-HT<sub>4</sub>R partial  
68 agonism/AChE inhibition,<sup>12</sup> H3R antagonism/VGCC block-  
69 ade,<sup>13</sup> GSK-3 $\alpha$ / $\beta$  inhibition/AChE inhibition,<sup>14</sup> NMDAR  
70 binding/AChE inhibition,<sup>15</sup> A<sub>1</sub>/A<sub>2A</sub>ARs blockade/MAO B  
71 inhibition,<sup>16</sup> AChE inhibition/MAO inhibition/H3R antago-  
72 nism,<sup>17</sup> among others) have been addressed as potential  
73 druggable options to treat AD with the use of multipotent  
74 small molecules.

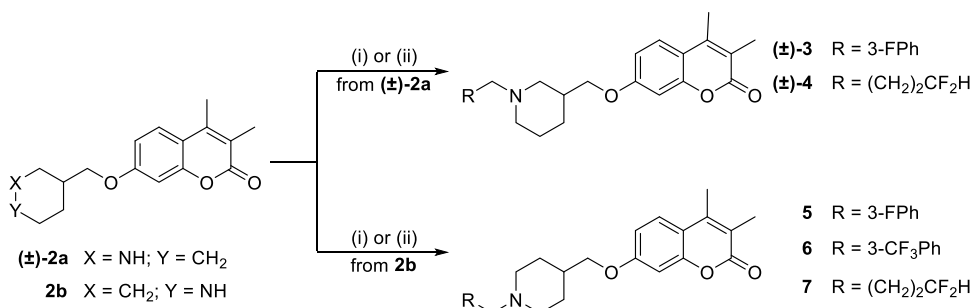
75 In this context, the old-fashioned dual inhibition of  
76 acetylcholinesterase (AChE) and monoamine oxidases  
77 (MAOs) is still an appealing research field.<sup>18–24</sup> The blockade  
78 of AChE activity contributes to an increased neurotransmitter  
79 level to counteract the depletion of cholinergic tone. Moreover,  
80 the occupancy of peripheral anionic subsite (PAS) with dual-  
81 binding-site AChE inhibitors can mitigate the  $\beta$ -amyloid  
82 aggregation rate.<sup>25</sup> On the other hand, brain MAO activity  
83 increases with ageing<sup>26</sup> and in cortex and hippocampus of AD  
84 patients;<sup>27,28</sup> thus, its inhibition can mitigate ROS production, in  
85 particular limiting hazardous species deriving from aldehydes  
86 and H<sub>2</sub>O<sub>2</sub> produced as catalytic cycle byproducts. After the

87 launch of ladostigil (Chart 1),<sup>29</sup> a dual inhibitor currently in  
88 clinical trials against mild cognitive impairment,<sup>30</sup> no other  
89 AChE-MAO inhibitor has joined the anti-Alzheimer drug  
90 discovery pipeline so far. However, this compound possesses a  
91 peculiar mechanism of action thanks to AChE pseudo-  
92 irreversible and MAO irreversible inhibition. Therefore,  
93 research is still needed to probe the effect of reversible  
94 compounds. After having largely explored the decoration of  
95 2H-chromen-2-one as a privileged scaffold<sup>31,32</sup> to develop  
96 potent dual and reversible AChE-MAO B inhibitors as original  
97 contribution to this field,<sup>18,19,33,34</sup> in the present work, we aimed  
98 at probing the effect of fluorinated motifs on both in vitro  
99 potency and druglike features of multimodal hit compounds  
100 already developed by us as potential agents against neuro-  
101 degenerative disorders.

102 Despite being slightly larger than hydrogen (van der Waals  
103 radius = 1.2 Å), covalently bound fluorine (1.47 Å) could  
104 strongly impact the molecular properties of drugs and druglike  
105 hit compounds as well. Since the early 1980s, the presence of  
106 fluorinated molecules has become routinely observed among  
107 newly marketed synthetic drugs.<sup>35</sup> Most properties raise from  
108 the highest electronegativity in the Pauling scale attributed to F  
109 (3.98), which could modulate pK<sub>a</sub> of nearby functional groups,  
110 increase the stability of proximal C–H bonds prone to  
111 oxidation, and affect binding energies with macromolecule  
112 targets by contributing direct multipolar contacts and/or  
113 tempering indirect dipolar interactions.<sup>36</sup> Usually, H/F  
114 exchange is envisaged to mitigate hepatic clearance and achieve  
115 higher bioavailability, particularly for orally administered drugs  
116 suffering from first-pass metabolism employing CYP enzymatic  
117 machinery.<sup>37</sup> To this extent, aromatic H/F isosteric mimicry is  
118 often pursued with the aim of decreasing C–H oxidation rates  
119 leading to *para*-hydroxylation without producing significant  
120 changes in binding free energies because of the size of F atom,  
121 rarely involved in steric clashes, and small contributions brought  
122 by lipophilic interactions (van der Waals, dipolar), provided that  
123 direct binding contacts with F and repulsive interactions are  
124 absent. Apart from (per)fluorinated alkanes, the introduction of  
125 F atom(s) increases the lipophilicity of parent compounds, thus  
126 affecting the physicochemical properties (solubility, membrane

Scheme 1. Synthesis of Gem-DifluoroIntermediate **1d**<sup>a</sup>

<sup>a</sup>Reagents and conditions: (i) benzoyl chloride, DIEA, acetonitrile, room temperature, 3 h, 92%; (ii) PCC, celite, an. CH<sub>2</sub>Cl<sub>2</sub>, room temperature, 21 h, 82%; (iii) DAST, an. CH<sub>2</sub>Cl<sub>2</sub>, 0 °C to room temperature, 1 h, 40%; (iv) (a) NaOCH<sub>3</sub>, trifluoroacetic acid, methanol, room temperature, 1.5 h; (b) NsCl, TEA, 4-(dimethylamino)pyridine, an. CH<sub>2</sub>Cl<sub>2</sub>, room temperature, 1.5 h, 38%.

Scheme 2. Synthesis of Piperidines **3–7**<sup>a</sup>

<sup>a</sup>Reagents and conditions: (i) for (**±**)-**3**, **5**, **6**: suitable benzyl bromide, K<sub>2</sub>CO<sub>3</sub>, acetonitrile, Δ, 5 h, 64–98%; (ii) for (**±**)-**4** and **7**: **1d**, K<sub>2</sub>CO<sub>3</sub>, acetonitrile, 80 °C, 18 h, sealed vessel, 46–51%.

permeability) and related pharmacokinetics (metabolic liabilities, nonspecific activities, target distribution).<sup>38</sup>

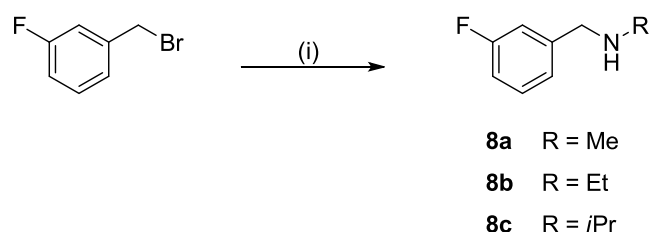
Indeed, fluorinated bioisosteres represent a useful, rapidly expanding tactic in medicinal chemistry useful to control target potency/selectivity, solubility, conformational bias, and pK<sub>a</sub> and temper metabolism, off-target distribution, and bioavailability. Ultimately successful drug discovery programs result from well-balancing all of these parameters. On account of this, herein, we employed fluorinated motifs to decorate diverse 2*H*-chromen-2-ones, previously reported as dual AChE-MAO B hits by some of us,<sup>18,33,34</sup> and we studied their impact over *in vitro* inhibitory activities and drug-likeness as well.

Since H/F substitution on aromatic rings could negatively affect aqueous solubility, we preferred to study only *meta*-positions (Figure 1, motif A), which could somehow disrupt symmetry and induce a lower lipophilicity penalty compared to more symmetric *para*-derivatives. Apart from H/F exchange on phenyl rings, the replacement of primary alcohols with difluoromethyl groups (CF<sub>2</sub>H) as weaker hydrogen-bonding (HB) donor bioisosteres was investigated (Figure 1, motif B and C).<sup>39</sup> CF<sub>2</sub>H groups make compounds more lipophilic than OH while maintaining HB ability though with lower acidity.<sup>40</sup> After *in vitro* biological evaluations toward target enzymes (ChEs and MAOs), the most interesting compounds were prioritized to assess physicochemical properties (solubility, lipophilicity, log *D*<sub>7,4μ</sub> membrane permeability) that are relevant for hit finding. Preliminarily, early-ADME profiling enclosed metabolic liability, brain penetration, and inherent cytotoxicity determination. In light of potent *in vitro* inhibitory data, nonfluorinated analogues were enrolled in drug-likeness study also for comparative purposes.

**Synthesis.** The preparation of difluoromethyl compounds required the synthesis of a common intermediate (**1d**) as illustrated in Scheme 1.<sup>41</sup> Commercially available 1,4-butanediol was mono-protected as benzoate followed by PCC (pyridinium chlorochromate)-mediated oxidation of **1a**. The nucleophilic fluorination of aldehyde **1b** was accomplished by (diethylamino)sulfur trifluoride (DAST) yielding benzoate **1c**, that was in

turn transformed into nosylate **1d**, as a better leaving group, by applying a two-step methanolysis/nosylation protocol. Nucleophilic substitution reactions coupling the suitable piperidine **2a–b**<sup>33</sup> with **1d** or suitable benzyl bromide as the electrophilic partner provided final compounds **3–7** (Scheme 2).

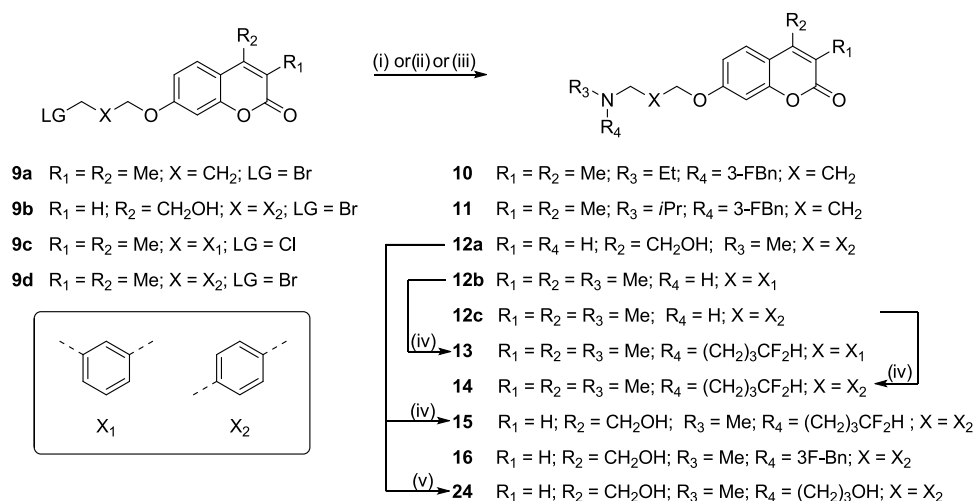
As indicated in Scheme 4, appropriate halides **9b–d** were reacted with excess methylamine yielding **12a–c** prior to final alkylation with **1d** to afford coumarins **13–15**. Compounds **10**, **11**, and **16** were obtained by heating intermediate bromides **9a–b** with suitable 3-*F*-substituted amine **8a–c** (Scheme 3) in refluxing acetonitrile or under microwave irradiation. The alkylation of **12a** with 3-bromo-1-propanol yielded non-fluorinated derivative **24** (Scheme 4).

Scheme 3. Synthesis of Intermediates **8a–c**<sup>a</sup>

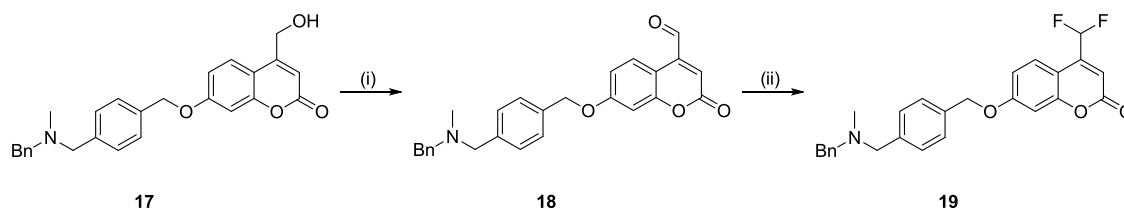
<sup>a</sup>Reagents and conditions: (i) CH<sub>3</sub>NH<sub>2</sub> (for **8a**) or CH<sub>3</sub>CH<sub>2</sub>NH<sub>2</sub> (for **8b**) or (CH<sub>3</sub>)<sub>2</sub>CHNH<sub>2</sub> (for **8c**), THF, room temperature, 6 h, 42–53%.

Scheme 5 illustrates the synthetic pathway leading to **19**. The procedure started from the controlled oxidation of alcohol **17** to aldehyde **18** in the presence of activated MnO<sub>2</sub> followed by DAST-promoted fluorination giving final compound **19**.

**Structure–Activity Relationships.** All coumarin derivatives in Table 1 were evaluated *in vitro* as inhibitors of target enzymes (*h*MAOs, *h*AChE, *h*sBChE) by applying kinuramine and Ellmann's assay<sup>42</sup> for MAOs<sup>18</sup> and ChEs,<sup>43</sup> respectively. Regarding the activity toward MAO isoenzymes, we aimed at achieving B/A selectivity to avoid well-known side effects linked to the inhibition of peripheral MAO A, termed “cheese effect”<sup>188</sup>

Scheme 4. Synthesis of Benzylamines 10, 11, 13–16, 24<sup>a</sup>

<sup>a</sup>Reagents and conditions: (i) for **10–11** (from **9a**): **8b** (for **10**) or **8c** (for **11**), K<sub>2</sub>CO<sub>3</sub>, KI (cat.), acetonitrile, Δ, 10 h, 30–80%; (ii) for **12a** (from **9b**), **12b** (from **9c**), **12c** (from **9d**): CH<sub>3</sub>NH<sub>2</sub>, THF, room temperature, 18 h, 75–93%; (iii) for **16** (from **9b**): **8a**, K<sub>2</sub>CO<sub>3</sub>, KI (cat.), acetonitrile, 130 °C, 30 min, MW, 61%; (iv) **1d**, K<sub>2</sub>CO<sub>3</sub>, acetonitrile, 80 °C, 18 h, sealed vessel, 42–50%; (v) 3-bromo-1-propanol, K<sub>2</sub>CO<sub>3</sub>, KI (cat.), acetonitrile, 80 °C, 4 h, sealed vessel, 34%.

Scheme 5. Synthesis of Coumarin 19<sup>a</sup>

<sup>a</sup>Reagents and conditions: (i) MnO<sub>2</sub>, an. CH<sub>2</sub>Cl<sub>2</sub>, room temperature, 2 h, 64%; (ii) DAST, an. CH<sub>2</sub>Cl<sub>2</sub>, 0 °C to room temperature, overnight, 16%.

189 from hypertensive crisis after tyramine-rich food consump-  
 190 tion.<sup>44</sup> On the other hand, selective AChE inhibition was not  
 191 considered a critical issue due to the increasing evidence that  
 192 highlighted the expedient targeting of BChE activity<sup>45</sup> in AD  
 193 brains as a promising therapeutic option.

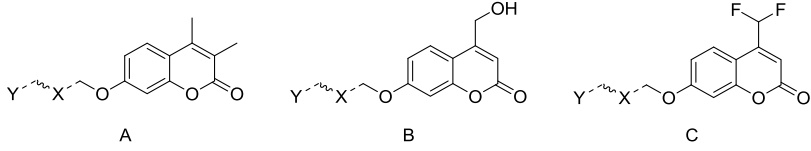
194 As inferred by in vitro inhibitory data obtained for *N*-  
 195 benzylpiperidines (**±**)-**3**, **5**, (**±**)-**21** and **23**, the introduction of  
 196 F-atom at the *meta*-position of phenyl rings exerted a negligible  
 197 impact on activity (MAO B IC<sub>50</sub>: from moderate to low  
 198 nanomolar; AChE IC<sub>50</sub>: from low micromolar to submicromo-  
 199 lar). More interestingly, the presence of *m*-F substitution did not  
 200 alter inhibitory trends markedly. With the exception of racemic  
 201 samples, whose MAO B inhibition was slightly enhanced by H/F  
 202 exchange (IC<sub>50</sub> for (**±**)-**3** = 12 nM, IC<sub>50</sub> for (**±**)-**21** = 30 nM), in  
 203 all cases, inhibitory activities were equipotent or slightly  
 204 worsened on both targets (compare (**±**)-**3** with (**±**)-**21**, **5**  
 205 with **23**). Moreover, the CF<sub>3</sub>-motif installed on compound **6** was  
 206 unable to improve binding interactions with MAO B as well as  
 207 AChE. Open chain derivatives **10–11** were designed to remove  
 208 chirality issues from analogue (**±**)-**3**. Ethyl-substituted **10** was a  
 209 better MAO B inhibitor than *i*Pr-derivative **11** (IC<sub>50</sub> = 73 and  
 210 350 nM, respectively), both being less active than parent  
 211 racemate (**±**)-**3**. On the other hand, AChE inhibition was not  
 212 affected by piperidine ring opening; thus, **10–11** showed low-  
 213 micromolar IC<sub>50</sub> values close to (**±**)-**3**. Looking at bis-  
 214 benzylamines, F-introduction in **16** was moderately tolerated  
 215 by AChE enzymatic cavity (IC<sub>50</sub> = 330 nM) as it produced a 3-  
 216 fold activity drop from **17** (IC<sub>50</sub> = 120 nM), whereas MAO B

inhibition remained untouched (IC<sub>50</sub> = 10 nM). Notwithstand-  
 ing, **16–17** were among the most interesting samples of the  
 whole series showing nanomolar dual-inhibitory potencies  
 toward AChE and MAO B, micromolar BChE inhibition, and  
 noteworthy B/A selectivity (SI > 1000).

Alcohol bioisosteric replacement based on CF<sub>2</sub>H as lipophilic  
 hydrogen-bonding donor produced a different activity trend in  
 chiral ((**±**)-**4** vs (**±**)-**20**) and achiral analogue (**7** vs **22**) pairs,  
 the latter showing close inhibitory potencies. A more remarkable  
 effect was retrieved upon comparing racemic **4** with **20**, since  
 CF<sub>2</sub>H-group improved MAO B and AChE inhibition by 6- and  
 2-fold, respectively, along with a slight activity increase against  
 MAO A.

The ring-pruning of the terminal phenyl group in **17** led to  
 more flexible and basic **13–15**, whose fluorinated alkyl chains  
 could mimic hydrophobic interactions performed by aromatic  
 cycle, at least in part. Thus, compounds **17** and **15** were  
 equipotent MAO B inhibitors, whereas a more considerable  
 difference was observed against AChE. *para*-substituted  
 derivative **14** displayed a better B/A selectivity than **13**, as a  
 consequence of lower MAO A inhibition and higher MAO B  
 potency. Restoring -CH<sub>2</sub>OH at coumarin C4 produced the  
 most active MAO B inhibitor (**15**, IC<sub>50</sub> = 8.2 nM), endowed  
 with outstanding selectivity (SI > 1250) along with strong and  
 selective potency against AChE (IC<sub>50</sub> = 550 nM). The CF<sub>2</sub>H  
 motif holds a key effect in profitably binding the hydrophobic  
 pockets of both MAO B and AChE, so much that alcohol-  
 bearing compound **24** returned a dramatic potency loss (IC<sub>50</sub> = 244

Table 1. Inhibition Data toward Target Enzymes for Compounds 3–7, 10–11, 13–17, 19–24



Cmpd	Gen. Struct.	Y	X	IC <sub>50</sub> (μM) or inhibition % at 10 μM <sup>a</sup>			
				<i>h</i> MAO-A <sup>b</sup>	<i>h</i> MAO-B <sup>b</sup>	<i>h</i> AChE <sup>c</sup>	<i>h</i> sBChE <sup>d</sup>
(±)-3	A			2.0±0.1	0.012±0.004	1.2±0.3	2.0±0.1
(±)-4	A			11±2	0.26±0.07	0.48±0.06	22±4%
5	A			2.5±0.1	0.14±0.03	0.46±0.10	2.9±0.2
6	A			1.4±0.2	0.13±0.02	0.47±0.07	35±4%
7	A			40±4%	0.53±0.11	1.2±0.1	8±2%
10	A			7.8±0.7	0.073±0.003	1.2±0.1	4.3±0.4
11	A			8.1±0.1	0.35±0.04	0.91±0.02	22±3%
13	A			4.2±0.2	0.56±0.01	1.7±0.1	1.6±0.1
14	A			45±3%	0.16±0.02	1.5±0.2	4.1±0.7
15	B			34±2%	0.0082±0.0019	0.55±0.07	34±2%
16	B			47±1%	0.010±0.003	0.33±0.04	1.1±0.1
17	B			15±2	0.010±0.002	0.12±0.01	1.1±0.3
19	C			17±3%	0.13±0.02	0.56±0.01	0.43±0.05
(±)-20	A			41±3%	1.5±0.1	1.1±0.1	26±3%
(±)-21	A			2.8±0.8	0.030±0.005	0.84±0.20	3.4±0.2
22	A			50±5%	0.48±0.05	0.89±0.12	30±3%
23	A			2.4±1.5	0.11±0.01	0.38±0.07	4.7±0.7
24	B			13±3%	0.42±0.06	2.2±0.1	27±4%
safinamide				20±3%	0.018±0.003	n.d.	n.d.
donepezil				n.d.	n.d.	0.023±0.003	2.1 ± 0.2

<sup>a</sup>Values are the mean of three independent experiments ± SEM. <sup>b</sup>Human recombinant MAOs on Supersomes. <sup>c</sup>Human AChE. <sup>d</sup>Horse serum BChE.

0.42 and 2.2 μM toward MAO B and AChE, respectively), likely caused by desolvation penalties.

Upon inserting bioisosteric CF<sub>2</sub>H-motif directly at position 4 of the coumarin ring, a stronger HBD group was expected as its acidity was strictly dependent on the EWG properties of the substituent attached to F-bound carbon atom.<sup>40</sup> Derivative 19, strongly lipophilic, proved to be a well-balanced pan-inhibitor for relevant targets (MAO B, AChE, and BChE; IC<sub>50</sub> = 132, 561, and 430 nM, respectively), showing good B/A selectivity (SI >

73) and the lowest IC<sub>50</sub> against BChE, at the submicromolar level.

**PAINS Evaluation.** Compounds under investigation were filtered by three in silico tools (ZINC15 pattern identifier,<sup>46</sup> PAINS remover,<sup>47</sup> FAF-Drugs4<sup>48</sup>) to identify potential Pan Assay Interference Compounds (PAINS)<sup>49</sup> linked to aggregating and/or undesirable structural scaffolds. Low risk was associated with the fluorescence of coumarins that could produce interferences with the kynuramine-based spectrofluorimetric protocol readouts. A direct spectrophotometric method,

measuring 4-hydroxyquinoline absorbance at 316 nm, although affected by lower sensitivity, was applied to the screening of some prototypes of hMAO B inhibitors (**5**, **11**, **15**, **16**). As reported in Table S1 (Supporting Information), IC<sub>50</sub> values were close to those obtained in fluorescence, thus excluding false positives among active compounds.

**Physicochemical and Early-ADME Profiling.** At the first stage, physicochemical profiling addressed kinetic aqueous solubility determination at a physiological pH (7.40) by means of UV or mass protocol. In addition, lipophilicity was assessed by determining log *D*<sub>7.4</sub> (LC-MS) as well as chromatographic hydrophobicity index (CHI) in a fast-gradient reversed-phase high-performance liquid chromatography (RP-HPLC) method, as indicated in Table 2.<sup>50</sup> The highest solubility values

pared to alcohols (CHI < 50). Within the water-soluble series of achiral compounds, **7** and **15** exhibited more favorable physicochemical properties compared to **22**, whose extreme polarity, among other structural factors, contributed an outstanding solubility along with experimental log *D*<sub>7.4</sub> value (0.84) quite lower than the calculated median (1.7) of marketed CNS drugs.<sup>51</sup> Indeed, the optimal extent (brain distribution) and rate (brain permeation through BBB) of central uptake depend on a well-balanced lipophilic/hydrophilic character. Moreover, the highly hydrophilic character for **22** could be associated with faster clearance.

After setting an arbitrary solubility threshold (20 μM), some derivatives were discriminated as poorly soluble and not progressed to permeation studies. Brain exposure to drugs depends on several mechanisms (distribution, BBB permeation, efflux-pumps liability) that often underlie the attrition rate for CNS-active agents. For orally administered drugs, adequate solubility and absorption from gastrointestinal (GI) tract is a prerequisite for CNS penetration. Parallel artificial membrane permeability assay on hexadecane membrane (PAMPA-HDM) support was applied to assess in vitro the ability of compounds to permeate intestinal epithelial barrier by passive diffusion, thus endorsing oral bioavailability (Table 3). Apart from non-fluorinated (±)-**21** and **23** (borderline low/moderate permeation) and **24** (low permeant), all derivatives enrolled in this assay were from moderate ((±)-**3**, **22**) to high permeant ((±)-**4**, **7**, **15**, (±)-**20**).

Drug disposition within CNS is restricted to molecules able to permeate BBB and evade efflux machinery arranged at the apical surface of endothelial cells shielding brain from xenobiotics. PAMPA protocol on porcine brain lipid extracts (PAMPA-PBLE) models BBB permeation by transcellular passive diffusion, the main mechanism used for exogenous small molecules brain uptake. Again, BBB penetration for (±)-**3**, (±)-**21**, and **23** was hampered by retention, whereas (±)-**4**, **7**, **15**, (±)-**20**, and **22** were predicted to passively permeate BBB and penetrate into CNS (Table 3), with **15** being the best performer. Derivative **24** displayed the lowest permeability, within the range of uncertainly permeant classification.

Even though permeation occurs, brain accumulation can be still prevented by efflux systems such as P-gp, one of the most expressed pumps extruding drugs at BBB level. To address this issue, a cell-based model employing Caco-2 lines provided intestinal permeability estimation along with P-gp liability evaluation as these transporters are expressed at the apical surface (Table 3). For all investigated compounds, bidirectional transport studies returned optimal ER values (<2) as the metric ruling out interactions with P-gp pump. Interestingly, fast permeability in both directions was scored by **15**, thus highlighting its well-balanced profile.

Metabolic stability is often a critical liability determining the success rate for medicinal chemistry programs, and transformations catalyzed by microsomal enzymes represent a major route for disposing of bioactive compounds (and their metabolites) through hepatic clearance thus affecting drug's bioavailability and half-life. Fluorine and F-containing motifs have been largely exploited as structural tools to encumber the activity of metabolizing enzymes, thanks to the niche of physicochemical properties (electronegativity, size, dipole moment, and bond-dissociation energy). In all compounds recruited for stability studies in mouse liver microsomes (MLM, see Table 4), the presence of EWG fluorinated groups on aromatic rings was unable to restore appreciable half-lives with

**Table 2. Physicochemical Properties of Compounds 3–7, 10–11, 13–17, 19–24**

cmpd	<i>S</i> (μM) <sup>a</sup>	log <i>D</i> <sub>7.4</sub> <sup>b</sup>	CHI <sub>pH7.4</sub> <sup>c</sup>
(±)- <b>3</b>	20 ± 3	4.38	>100
(±)- <b>4</b>	349 ± 5	2.67	83.4
<b>5</b>	11.0 ± 0.5	3.43	>100
<b>6</b>	0.9 ± 0.3 <sup>d</sup>	5.05	>100
<b>7</b>	448 ± 12	2.34	73.4
<b>10</b>	18 ± 2	n.d. <sup>e</sup>	>100
<b>11</b>	13 ± 1	n.d. <sup>e</sup>	>100
<b>13</b>	13 ± 1	3.65	>100
<b>14</b>	13 ± 1	3.78	>100
<b>15</b>	201 ± 11	2.48	76.4
<b>16</b>	2.4 ± 0.1 <sup>d</sup>	4.29	>100
<b>17</b>	13 ± 1	3.81	99.3
<b>19</b>	0.40 ± 0.04 <sup>d</sup>	4.80	>100
(±)- <b>20</b>	>500	1.15	48.8
(±)- <b>21</b>	33 ± 2	3.65	>100
<b>22</b>	>500	0.86	47.3
<b>23</b>	57 ± 4	3.40	99.7
<b>24</b>	>500	n.d. <sup>e</sup>	35.6

<sup>a</sup>Kinetic solubility measured in PBS (pH 7.4) by UV–vis spectrophotometry from triplicate experiments. Values are the mean of three independent experiments ± SEM. <sup>b</sup>1-Octanol/PBS (pH = 7.4) distribution coefficients determined through the shake-flask method. Compound concentration was measured by HPLC-ES-MS/MS. <sup>c</sup>Chromatographic hydrophobicity index determined through a fast-gradient reversed-phase HPLC method. Values > 100 were not exactly indicated as they are outside the linearity range compared to retention time. <sup>d</sup>HPLC/MS analysis for sensitivity reasons. <sup>e</sup>Not determined.

(>500 μM) were returned by alcohols (±)-**20**, **22**, and **24**, whereas both basicity attenuation and lipophilicity increase induced by benzyl group in (±)-**21** and **23** worsened solubility and partitioning parameters.

As expected, the presence of F-arene moieties enhanced hydrophobicity indexes; thus, compounds (±)-**3**, **5**, **10**, **11** displayed inadequate solubility (11 μM < Sol < 20 μM) for further development along with adverse distribution coefficients, even worsened by –CF<sub>3</sub> group (**6**). Bis-benzylamines **16–17** suffered from critical *S* values, affected by lower protonation degree at pH 7.4, as well as benzylamines **13–14**. Among fluorinated derivatives, more favorable physicochemical properties (solubility > 200 μM, CHI < 85, log *D*<sub>7.4</sub> < 3) were restored by modulating p*K*<sub>a</sub> in *N*-alkylpiperidines (±)-**4** and **7**, and by polar substituents at coumarin C4 (**15**) even though difluoromethyl groups determined a lipophilic penalty com-

Table 3. Permeation Studies of Selected Compounds

compd	PAMPA-HDM <sup>a</sup>	PAMPA-BBB <sup>b</sup>		CACO-2 $P_{app}$ ( $\times 10^{-5}$ cm/s) <sup>c</sup>		
	$\log P_a$ (cm/s)	$P_e$ ( $\times 10^{-6}$ cm/s)	classification	A $\rightarrow$ B	B $\rightarrow$ A	ER
( $\pm$ )-3	$-4.8 \pm 0.01$	$10.0 \pm 3.0$	retention			
( $\pm$ )-4	$-4.2 \pm 0.04$	$13.3 \pm 3.9$	CNS +			
7	$-4.2 \pm 0.07$	$10.8 \pm 1.2$	CNS +	$1.7 \pm 0.6$	$1.6 \pm 0.1$	1.0
15	$-4.4 \pm 0.05$	>14	CNS +	$2.5 \pm 0.1$	$1.6 \pm 0.2$	0.6
( $\pm$ )-20	$-4.4 \pm 0.01$	$7.2 \pm 0.8$	CNS +			
( $\pm$ )-21	$-5.0 \pm 0.02$		retention			
22	$-4.7 \pm 0.04$	$6.0 \pm 0.1$	CNS +	$1.9 \pm 1.0$	$2.2 \pm 0.7$	1.2
23	$-5.0 \pm 0.16$		retention	$0.7 \pm 0.2$	$1.2 \pm 0.7$	1.6
24	<-6.5	$3.1 \pm 0.1$	CNS +/-			

<sup>a</sup>Parallel Artificial Membrane Permeation Assay with a hexadecane artificial membrane. Values are mean  $\pm$  SD from duplicates. <sup>b</sup>Parallel Artificial Membrane Permeation Assay with Porcine Brain Lipid Extract (PBLE) dissolved in dodecane layer on a PVDF membrane support. Values are mean  $\pm$  SD from duplicates. <sup>c</sup>Apparent permeability across Caco-2 cells monolayer. A  $\rightarrow$  B: apical to basolateral direction. B  $\rightarrow$  A: basolateral to apical direction. ER: efflux ratio =  $P_{app}$  B  $\rightarrow$  A /  $P_{app}$  A  $\rightarrow$  B.

Table 4. Microsomal Stability, Clearance, and Inhibition of Human CYP3A4

compd	microsomal stability <sup>a</sup> $t_{1/2}$ (min)		$CL_{int}$ <sup>b</sup>		CYP3A4 ( $IC_{50}$ , $\mu M$ ) <sup>c</sup>
	mouse	human	mouse	human	
( $\pm$ )-3	$6.6 \pm 0.1$		$209.8 \pm 0.1$		
( $\pm$ )-4	$17.8 \pm 0.5$		$78.1 \pm 4.2$		>10
5	$6.2 \pm 0.2$		$224.9 \pm 7.7$		
6	$9.5 \pm 0.3$		$146.4 \pm 4.3$		
7	$11.9 \pm 1.2$	$98.9 \pm 4.1$	$116.3 \pm 11.5$	$14.1 \pm 0.6$	$0.8 \pm 0.1$
10	$5.3 \pm 0.8$		$260.4 \pm 36.2$		
13	$4.8 \pm 0.9$		$288.6 \pm 9.4$		$0.6 \pm 0.1$
15	$25.0 \pm 2.8$	$34.9 \pm 0.9$	$55.6 \pm 6.2$	$39.8 \pm 1.0$	$10 \pm 2$
16	$36.9 \pm 2.2$		$37.7 \pm 2.3$		$3.5 \pm 0.6$
17	$31.7 \pm 0.1$		$43.9 \pm 0.1$		$7 \pm 1$
19	$9.8 \pm 0.1$		$141.9 \pm 0.9$		
( $\pm$ )-20	$92.4 \pm 12.6$		$15.1 \pm 3.1$		
( $\pm$ )-21	$5.3 \pm 0.1$		$264.7 \pm 4.5$		
22	$47.2 \pm 3.2$	>120	$29.5 \pm 1.9$	<11.5	>10
23	$6.7 \pm 0.2$		$206.3 \pm 6.7$		
ketoconazole					$0.025 \pm 0.003$

<sup>a</sup>Values are mean  $\pm$  SD from duplicates. <sup>b</sup>Intrinsic clearance expressed in  $\mu L / (\text{min} \times \text{mg})$  protein. Values are mean  $\pm$  SD from duplicates. <sup>c</sup>Recombinant CYP450 proteins used in a fluorescent homogeneous assay. Values are mean  $\pm$  SD from triplicates.

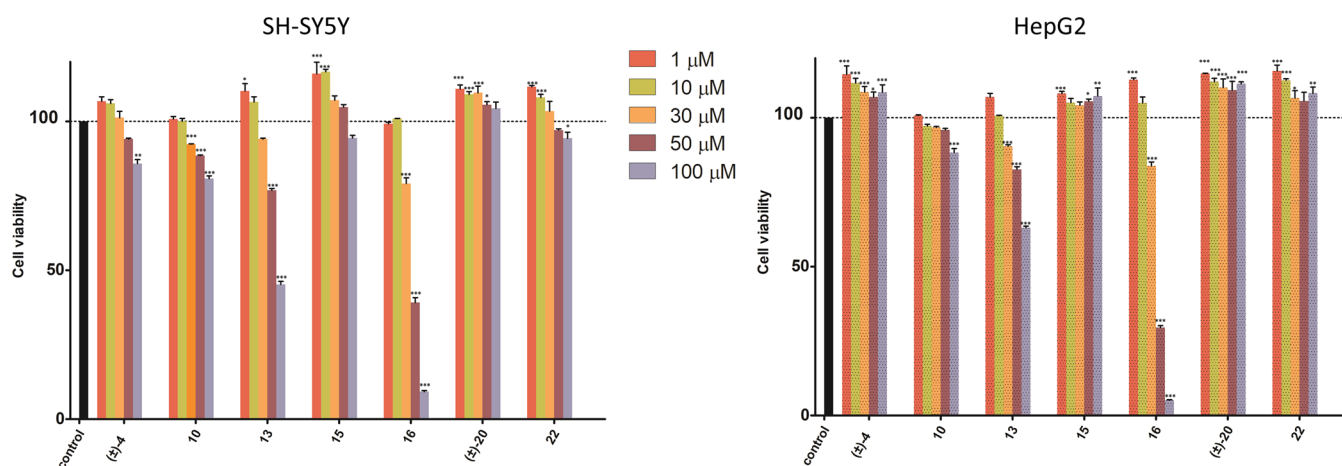
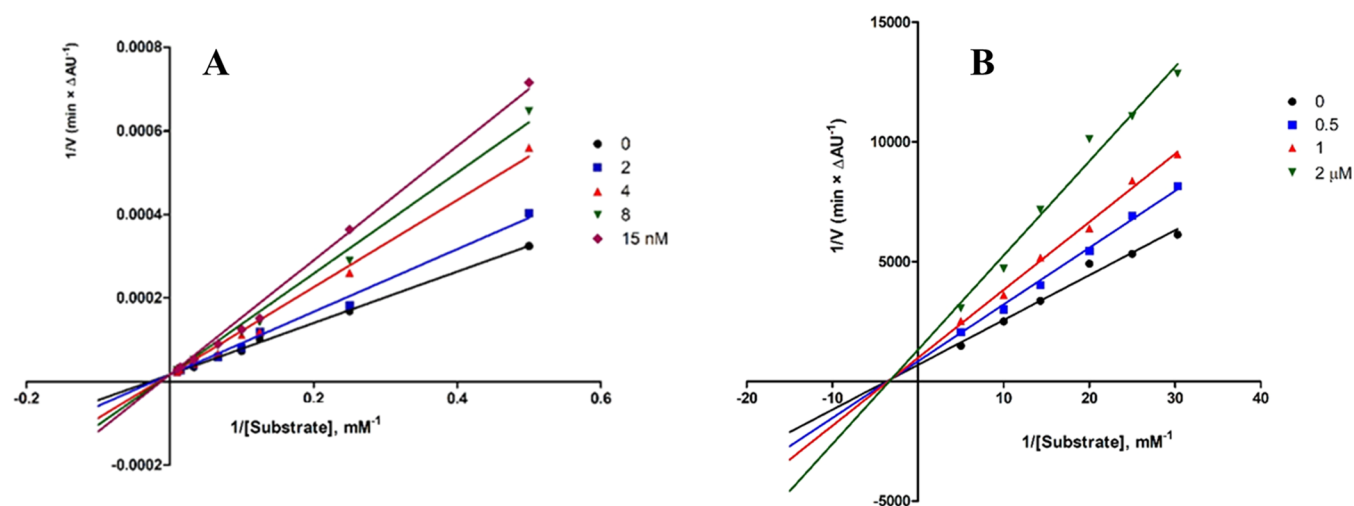


Figure 2. Viability of SH-SY5Y and HepG2 cells in the presence of compounds ( $\pm$ )-4, 10, 13, 15-16, ( $\pm$ )-20, and 22 at different concentrations measured through CellTiter-Glo Luminescent Cell Viability Assay and showed as mean  $\pm$  SD of three independent experiments, each performed in triplicate and referred to untreated control cells (control, 100% values, in the absence of compound). Statistical significance was calculated using a two-way analysis of variance (ANOVA) followed by the Bonferroni post hoc tests (GraphPad Prism version 5); \* $p$  < 0.05, \*\* $p$  < 0.01, \*\*\* $p$  < 0.001.



**Figure 3.** Lineweaver–Burk plots of inhibition kinetics for compound **15** toward *h*MAO B (A) and *h*AChE (B). Reciprocals of enzyme activity vs reciprocals of substrates' concentration in the presence of different inhibitor's concentrations (0–15 nM for *h*MAO B, 0–2  $\mu$ M for *h*AChE; reported in insets).

357 respect to unsubstituted analogues (( $\pm$ )-**21** vs ( $\pm$ )-**3**, **5–6** vs  
 358 **23**), ruling out hot spots in this region reliably. As could be  
 359 expected, more lipophilic  $-\text{CF}_2\text{H}$  bioisostere produced higher  
 360 clearance in mouse microsomal preparations, making com-  
 361 pounds **7** and ( $\pm$ )-**4** much more labile than alcohols **22** and  
 362 ( $\pm$ )-**20**, respectively. Interestingly, compounds bearing a  
 363  $-\text{CH}_2\text{OH}$  group at coumarin C4 did not suffer from metabolic  
 364 liabilities, even tempered by *meta*-F substitution (**16–17**;  $t_{1/2}$  =  
 365 36.9 and 31.7 min, respectively). Given the potent in vitro  
 366 inhibitory activities along with favorable preliminary phys-  
 367 icochemical and permeation features displayed by **7**, **15**, and **22**,  
 368 these compounds were also tested in human liver microsomes  
 369 (HLM). Even more surprisingly, fluorinated **7** showed greatly  
 370 enhanced half-life when tested in human liver microsomes,  
 371 though confirming its higher instability than parent **22** (>120  
 372 min). The high metabolic stability of dual hit **15** in MLM ( $t_{1/2}$  =  
 373 25 min,  $\text{CL}_{\text{int}} = 55.6 \mu\text{L}/(\text{min} \times \text{mg})$  protein) endorsed its  
 374 remarkable druglike profile, exhibiting also lower clearance in  
 375 HLM ( $t_{1/2} = 34.9$  min,  $\text{CL}_{\text{int}} = 39.8 \mu\text{L}/(\text{min} \times \text{mg})$  protein).  
 376 Very often, adverse effects coming from co-administered  
 377 drugs are the consequence of inhibited metabolic machinery  
 378 involving cytochromes within hepatocytes. Being one of the five  
 379 major isoforms, CYP3A4 was used to probe the chance of drug–  
 380 drug interactions related to metabolism blockade. At a first  
 381 glance, no clear correlation between inhibition of CYP3A4 and  
 382 structural motifs (or related physicochemical parameters) could  
 383 be envisaged for the subset displayed in Table 4. For instance,  
 384 both derivatives **15** and **22** behaved as weak CYP3A4 inhibitors,  
 385 suggesting that their slow metabolic clearance is unrelated to  
 386 self-inhibiting metabolic processes, whereas a close congener of  
 387 **15** (compound **13**) was found as a potent inhibitor.  
 388 Interestingly, strong CYP3A4 inhibition ( $\text{IC}_{50} = 0.8 \mu\text{M}$ )  
 389 might account, at least in part, for the much greater metabolic  
 390 stability displayed by compound **7** in HLM than in MLM.

391 Both tissue-specific and nonspecific cytotoxicities were  
 392 studied by measuring the effect on cell viability (ATP detection  
 393 assay with respect to control, in the absence of compounds)  
 394 upon co-incubating selected samples with human neuro-  
 395 blastoma (SH-SY5Y) and hepatocarcinoma (HepG2) cell  
 396 lines as prototypes for neuronal and hepatic cells, respectively.  
 397 As displayed in Figure 2, most compounds were devoid of

cytotoxic effects also at the highest concentrations applied (100  $\mu\text{M}$ ). Both alcohols ( $\pm$ )-**20** and **22** did not impair cell viability in both cultures, whereas, among fluorinated derivatives, **15** demonstrated the safest profile showing only negligible alteration of viable SH-SY5Y cells when assayed at 100  $\mu\text{M}$  along with nontoxic activity at all against HepG2 lines. The only exception was represented by coumarin **16**, whose moderate cellular damage returned  $\text{IC}_{50} = 40 \mu\text{M}$  in both lines.

**Investigation of Hit Compound 15.** In light of preliminary physicochemical and early-ADME data profiling, achiral  $\text{CF}_2\text{H}$ -bearing coumarin **15** emerged as a hit compound endowed with potent in vitro dual AChE-MAO B inhibition along with the most promising metabolic, physicochemical, safety, and CNS-distribution features.

**Inhibition Kinetics.** The kinetics of inhibition of compound **15** was studied toward both target enzymes (*h*MAO B and *h*AChE). As inferred from Figure 3A, coumarin **15** behaved as a competitive *h*MAO B inhibitor with  $K_i = 13 \pm 2$  nM. To shed light on the mechanism of action, the residual enzymatic activity was studied in a time-course experiment, with and without preincubating the enzyme in the presence of the inhibitors (Figure S2). Derivative **15** (10 nM) showed the same time-course evolution in both experiments, unrelated to preincubation. A close behavior was performed by safinamide (10 nM), a well-known reversible MAO B inhibitor. On the contrary, pargyline (100 nM) fully blocked enzymatic activity upon 1 h preincubation as for covalent irreversible propargylamine inhibitors. Regarding AChE inhibition kinetics, Lineweaver–Burk plots in Figure 3B were typical of a mixed-mode inhibition ( $K_i = 2.0 \pm 0.3 \mu\text{M}$ ) and suggested partial PAS occupancy for **15** as expected for dual-binding site AChE inhibitors.

**Neuroprotection Studies.** After ensuring the absence of inherent cytotoxicity induced by derivative **15** on neuroblastoma line at the concentrations under study, 3-(4,5-dimethylthiazol-2-yl)-2,5-diphenyl-tetrazolium bromide (MTT) assay was applied to determine the percentage of viable cells co-incubated with **15** and three different insults, namely, hydrogen peroxide ( $\text{H}_2\text{O}_2$ , 50  $\mu\text{M}$ , 4A),  $\beta$ -amyloid ( $A\beta_{1-42}$ , 20  $\mu\text{M}$ , 4B), and *N*-methyl-D-aspartate (NMDA, 250 and 500  $\mu\text{M}$ , 4C). Even if lower than standard quercetin (used as positive control), the neurorescue ability of **15** against pro-oxidant  $\text{H}_2\text{O}_2$



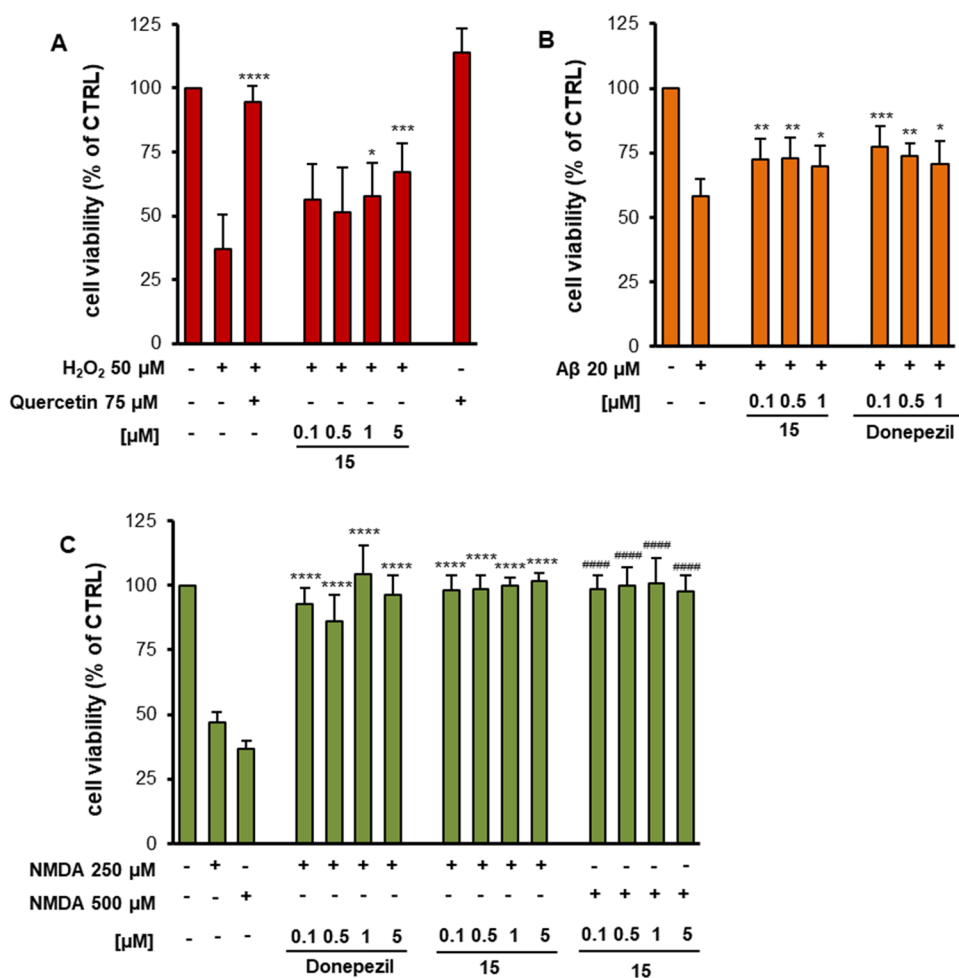


**Figure 4.** Effect of compound **15** at 0.1–5 μM concentrations on viable SH-SY5Y cells in the absence and presence of toxic insults (H<sub>2</sub>O<sub>2</sub>, 50 μM, A; Aβ<sub>1-42</sub>, 20 μM, B; NMDA, 250 and 500 μM, C) after co-incubation for 24 h. Viability was measured through MTT test and is shown as mean ± SD of three independent experiments, each performed in triplicate and referred to untreated control cells (CTRL, 100% values). Quercetin (75 μM) and donepezil (0.1–5 μM) were used as positive controls, as standard antioxidant and anti-AD reference drug, respectively. Statistical analysis was done by applying one-way ANOVA followed by multiple comparison tests (Dunnett's test). Levels of significance: \*\*\*\**p* < 0.0001, \*\*\**p* < 0.001, \*\**p* < 0.01, \**p* < 0.05, #####*p* < 0.0001.

439 (co-incubated at 50 μM) was statistically significant at 1 and 5  
 440 μM. Moreover, a significant cytoprotective effect against Aβ<sub>1-42</sub>  
 441 toxicity was shown in the 0.1–1 μM range (Figure 4B). Finally,  
 442 this compound greatly increased the number of viable cells  
 443 insulted by NMDA, fully neutralizing the cytotoxic effect of the  
 444 insult (250–500 μM) also when co-incubated at nanomolar  
 445 concentration, as shown in Figure 4C. Interestingly, the  
 446 protective activity was comparable to that of donepezil at the  
 447 same concentrations, used as a standard anti-Alzheimer drug.

448 **Albumin Binding.** The evaluation of human serum albumin  
 449 (HSA) binding for **15** and nonfluorinated congener **22**, for  
 450 comparative purposes, was performed by surface plasmon  
 451 resonance (SPR) using warfarin as a reference compound.<sup>52,53</sup>  
 452 Being the most abundant plasma protein, HSA binding can  
 453 deeply influence drug bioavailability and then plays a central role  
 454 in the ADME profile of xenobiotics. Indeed, the estimation of  
 455 HSA affinity can be assessed in the earlier steps of hit discovery.  
 456 The association (*k*<sub>on</sub>) and dissociation (*k*<sub>off</sub>) rate constants  
 457 resulted too fast to be calculated with good approximation, and  
 458 both **15** and **22** can be considered as fast and reversible HSA  
 459 binders. They further resulted as moderate HSA binders,  
 460 showing *K*<sub>D</sub> = 31.7 and 11.3 μM for **22** and **15** (Figure S3),  
 461 respectively, higher than reference warfarin (*K*<sub>D</sub> = 5.5 μM),

462 considered a strong HSA binder.<sup>54</sup> Interestingly, derivative **15**  
 463 (*K*<sub>D</sub> = 11.3 μM) bearing a difluoromethyl group, as more  
 464 lipophilic and weaker hydrogen-bonding (HB) donor bio-  
 465 isostere for hydroxyl, showed HSA affinity 3-fold higher than  
 466 alcohol **22** (*K*<sub>D</sub> = 31.7 μM). However, at a physiological HSA  
 467 plasma concentration (about 680 μM), compound **15** (at 10 μM  
 468 concentration) was predicted to achieve 20–40% albumin  
 469 binding, thus returning good bioavailability.

470 **Molecular Docking Simulations.** Molecular docking  
 471 simulations were carried out to shed light on binding poses  
 472 played by **15** within target enzymes. Human AChE and MAO B  
 473 coded as 4EY7 and 2VSZ, respectively, were retrieved from  
 474 Protein Data Bank (PDB). Regarding hAChE (Figure 5A), the  
 475 coumarin core of **15** packed against PAS, where it was anchored  
 476 through a face-to-face arene-arene interaction occurring with  
 477 Trp286, and a hydrogen-bonding network involving the lateral  
 478 CH<sub>2</sub>OH chain. The binding was further stabilized by additional  
 479 π–π stacking between the aromatic linker and the side chain of  
 480 Tyr341 lining the mid-gorge in an open conformation. Bridge  
 481 flexibility allowed the basic chain to fit catalytic anionic subsite  
 482 (CAS), by means of the positively charged amine interacting  
 483 with both the indole ring of Trp86 and Tyr337 side chain, and to  
 484 orient the fluorinated chain toward the oxyanionic hole. The

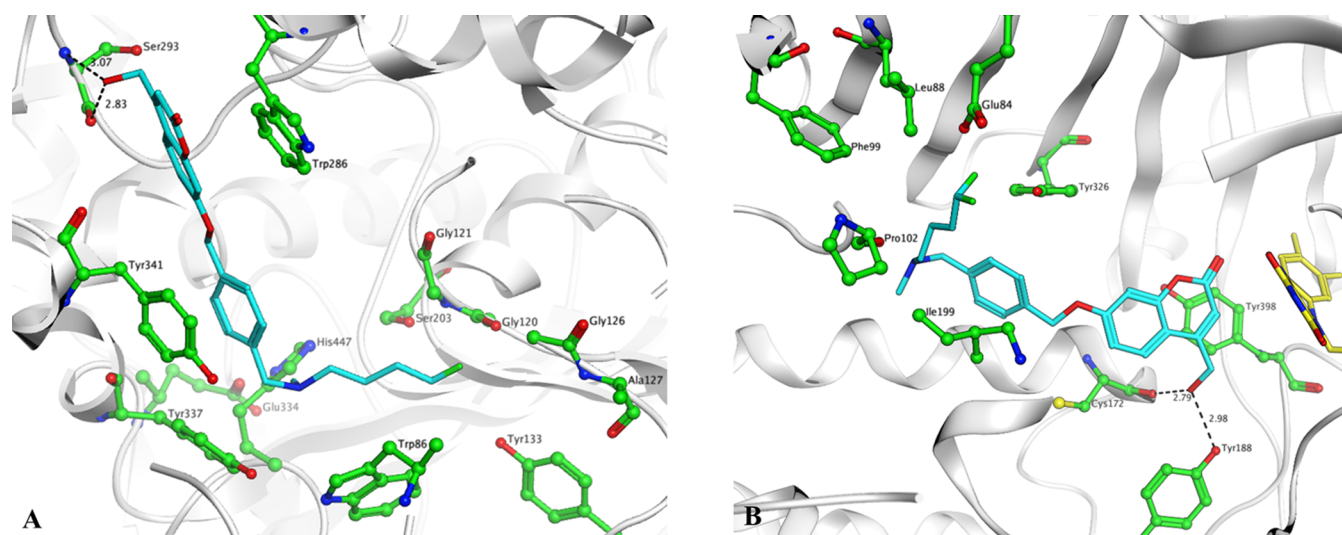


**Figure 5.** Top-scored binding poses of compound **15** docked within *hAChE* (A, PDB 4EY7,  $-10.79$  kcal/mol) and *hMAO B* (B, PDB 2V5Z,  $-10.88$  kcal/mol). Ligand is rendered as sticks, relevant amino acid residues are rendered as ball and sticks, while protein is represented as a cartoon. Colors are in accordance with the atom code, C atoms in cyan and green for ligand and amino acid, respectively. Residues forming AChE catalytic triad (Glu334-His447-Ser203) are rendered as semitransparent ball and sticks (6A). Carbon atoms of FAD coenzyme in human MAO B are colored in yellow and depicted as sticks (6B). Dotted lines represent HB.

burying of the inhibitor within the active site, fully occupied from PAS to CAS, was in agreement with the mixed-mode kinetics returned by **15**. The binding pose within MAO B is illustrated in Figure 5B, showing the inhibitor fully buried within the enzymatic cavity lined by aromatic residues. The coumarin is accommodated close to FAD stacking in front of Tyr398 ( $\pi$ - $\pi$  interaction) and Tyr188 through a bidentate HB with phenolic OH and Cys172 carbonyl. The flipping of the xylyl linker permitted a molecular folding that escaped steric clashes with gating Ile199, upon interacting with Tyr326, whereas the aliphatic chain pointed at outer regions. Even if the lipophilic CF<sub>2</sub>H motif seems unable to provide direct binding contacts, its contribution to affinity could arise from a more favorable desolvation effect compared to less active nonfluorinated analogue **24**.

## 500 ■ CONCLUSIONS

As a part of our ongoing research aimed at discovering neuroprotective dual AChE-MAO B inhibitors, here, we exploited H/F and CH<sub>2</sub>OH/CF<sub>2</sub>H bioisosteric replacement to develop novel coumarin-based multitarget inhibitors. Given that the introduction of fluorine and fluorinated motifs could strongly modulate relevant properties (binding affinity, basicity, bioavailability, metabolic stability) for medicinal chemistry research, in vitro screening toward target enzymes was followed by drug-likeness evaluation enrolling the most promising hits, hierarchically advanced to each step of early-ADME profiling that addressed solubility, CNS penetration, cytotoxicity, bioavailability predictors (metabolic stability, albumin binding, Caco-2 permeation). Fluorinated motifs (F/CF<sub>2</sub>H) were mostly tolerated by target enzymes without affecting inhibitory potency at a remarkable level compared to parent nonfluorinated compounds, with few exceptions ( $(\pm)$ -**4** vs  $(\pm)$ -**20**, **15** vs **24**) whose dual activity gain could be ascribed to CF<sub>2</sub>H. As expected, fluorine more deeply influenced physicochemical properties (solubility, lipophilicity), whereas cytotoxicity, CNS-distribution, and microsomal stability were affected to a lesser extent.

In this work, compound **15** displayed outstanding in vitro targets' inhibition (IC<sub>50</sub> = 550 and 8.2 nM for AChE and MAO B, respectively). Even if no specific direct binding interactions with F were retrieved in docking analysis, from an entropy viewpoint CF<sub>2</sub>H/CH<sub>2</sub>OH replacement likely contributed a more favorable desolvation effect compared to alcohol **24**. In addition, **15** showed a promising druglike character taking advantage of an optimal hydrophilic/lipophilic balance allowed by CF<sub>2</sub>H motif as a weak and lipophilic HB donor. This coumarin showed high solubility and brain-permeant features. The oral bioavailability of **15** was strongly supported by poor drug-drug interaction liability, good metabolic stability, moderate binding to plasma albumin, fast transport across Caco-2 lacking P-gp efflux. In SH-SY5Y and HepG2 cell lines, **15** produced negligible cytotoxic effects. Moreover, it was able to reduce the neuronal damage produced by both A $\beta$ <sub>1-42</sub> and H<sub>2</sub>O<sub>2</sub>, and to fully switch off NMDA toxicity in neuroblastoma culture. In light of these preliminary data, this compound will deserve further evaluation in preclinical in vivo pharmacokinetic studies and then in AD animal models to validate its neuroprotective efficacy, after scaling up and optimizing the synthesis with the aim of reducing the impact of hazardous DAST.

## 544 ■ EXPERIMENTAL SECTION

**Chemistry.** Starting materials, reagents, and analytical grade solvents were purchased from Sigma-Aldrich, Alfa-Aesar or Fluorochem (Europe). The purity of all of the intermediates, checked by RP-HPLC, was always better than 95%. RPLC analyses were performed on an Analytic Agilent 1260 Infinity multidetector system equipped with an automatic sampler and a 1200 series UV-diode array detector using a Kinetex 2.6 mm C18 column (150 mm  $\times$  2.1 mm I. D.). UV detection was measured at 230, 254, 280, and 320 nm. Each tested compound was analyzed by isocratic elution with two different mobile phase systems: in system 1, compounds were eluted using a 70/30 methanol/ammonium formate buffer (10 mM, pH 4.5) mixture at a flow rate of 0.2 or 0.5 mL/min; in system 2, compounds were eluted using a 65/35 acetonitrile/ammonium formate buffer (10 mM, pH 4.5) mixture at a flow rate of 0.2 or 0.5 mL/min. All of the newly prepared and tested compounds showed purity higher than 95% (elemental

560 analysis). Elemental analyses were performed on the EuroEA 3000  
561 analyzer only on the final compounds tested as MAOs and ChEs  
562 inhibitors. The measured values for C, H, and N agreed to within  $\pm$   
563 0.40% of the theoretical values. Microwave reactions were performed in  
564 a Milestone MicroSynth apparatus, setting temperature and hold times,  
565 fixing maximum irradiation power to 500 W and heating ramp times to  
566 2 min. Column chromatography was performed using Merck silica gel  
567 60 (0.063–0.200 mm, 70–230 mesh). Flash chromatographic  
568 separations were performed on Biotage SP1 purification system using  
569 flash cartridges prepacked with KP-Sil 32–63  $\mu$ m, 60 Å silica. All  
570 reactions were routinely checked by thin-layer chromatography (TLC)  
571 using Merck Kieselgel 60 F<sub>254</sub> aluminum plates and visualized by UV  
572 light. Regarding the reaction requiring the use of dry solvents, the  
573 glassware was flame-dried and then cooled under a stream of dry argon  
574 before the use. Nuclear magnetic resonance spectra were recorded on a  
575 Varian Mercury 300 instrument (at 300 MHz) or on an Agilent  
576 Technologies 500 apparatus (at 500 MHz) at ambient temperature in  
577 the specified deuterated solvent. Chemical shifts ( $\delta$ ) are quoted in parts  
578 per million (ppm) and are referenced to the residual solvent peak. The  
579 coupling constants  $J$  are given in hertz (Hz). The following  
580 abbreviations were used: s (singlet), d (doublet), dd (doublet of  
581 doublet), ddd (doublet of doublet of doublet), t (triplet), q  
582 (quadruplet), qn (quintuplet), m (multiplet), br s (broad signal);  
583 signals due to OH and NH protons were located by deuterium  
584 exchange with D<sub>2</sub>O. HRMS experiments were performed with a dual  
585 electrospray interface (ESI) and a quadrupole time-of-flight mass  
586 spectrometer (Q-TOF, Agilent 6530 Series Accurate-Mass Quadrupole  
587 Time-of-Flight LC/MS, Agilent Technologies Italia S.p.A., Cernusco  
588 sul Naviglio, Italy). Full-scan mass spectra were recorded in the mass/  
589 charge ( $m/z$ ) range 50–3000 Da. Melting points for solid final  
590 compounds were determined by the capillary method on a Stuart  
591 Scientific SMP3 electrothermal apparatus and are uncorrected. The  
592 following compounds have been already described in the literature: 4-  
593 hydroxybutyl benzoate **1a**,<sup>55</sup> 3,4-dimethyl-7-(piperidin-3-ylmethoxy)-  
594 2H-chromen-2-one **2a**,<sup>33</sup> 3,4-dimethyl-7-(piperidin-4-ylmethoxy)-2H-  
595 chromen-2-one **2b**,<sup>33</sup> [(3-fluorobenzyl)piperidin-3-yl]methoxy-3,4-  
596 dimethyl-2H-chromen-2-one ( $\pm$ )-**3**,<sup>56</sup> 7-(3-bromopropoxy)-3,4-di-  
597 methyl-2H-chromen-2-one **9a**,<sup>57</sup> 7-[[4-(bromomethyl)benzyl]oxy]-4-  
598 (hydroxymethyl)-2H-chromen-2-one **9b**,<sup>34</sup> 7-((3-(chloromethyl)-  
599 benzyl)oxy)-3,4-dimethyl-2H-chromen-2-one **9c**,<sup>18</sup> 7-((4-  
600 (bromomethyl)benzyl)oxy)-3,4-dimethyl-2H-chromen-2-one **9d**,<sup>18</sup> 7-  
601 [1-7-[(4-[[benzyl(methyl)amino]methyl]benzyl)oxy]]-4-(hydroxy-  
602 methyl)-2H-chromen-2-one **17**,<sup>34</sup> 7-[[1-(3-hydroxypropyl)piperidin-  
603 3-yl]methoxy]-3,4-dimethyl-2H-chromen-2-one ( $\pm$ )-**20**,<sup>18</sup> 7-[[1-(benzyl-  
604 zylpiperidin-3-yl)methoxy]-3,4-dimethyl-2H-chromen-2-one  
605 ( $\pm$ )-**21**,<sup>33</sup> 7-[[1-(3-hydroxypropyl)piperidin-4-yl]methoxy]-3,4-di-  
606 methyl-2H-chromen-2-one **22**,<sup>18</sup> 7-[[1-(benzylpiperidin-4-yl)-  
607 methoxy]-3,4-dimethyl-2H-chromen-2-one **23**.<sup>33</sup>

608 **4-Oxobutyl benzoate (1b)**. A solution of **1a**<sup>55</sup> (23 mmol, 4.5 g) in  
609 anhydrous CH<sub>2</sub>Cl<sub>2</sub> (15 mL) was dropped into a stirred suspension of  
610 pyridinium chlorochromate (PCC) (35 mmol, 7.4 g) and celite (8 g) in  
611 dry CH<sub>2</sub>Cl<sub>2</sub> (50 mL) in a two-neck round-bottom flask. The resulting  
612 dark brown mixture was kept at room temperature for 1.5 h and then  
613 diluted with anhydrous Et<sub>2</sub>O (180 mL) and filtered through a celite  
614 pad. The solvents were evaporated under reduced pressure and the  
615 crude residue was purified by flash chromatography (gradient eluent:  
616 ethyl acetate in *n*-hexane, 0  $\rightarrow$  20%) to give the pure aldehyde **1b** as a  
617 colorless oil. Yield: 82%. <sup>1</sup>H NMR (500 MHz, CDCl<sub>3</sub>)  $\delta$ : 9.84 (s, 1H),  
618 8.02 (ddd,  $J$  = 8.5, 3.4, 1.4 Hz, 2H), 7.63–7.52 (m, 1H), 7.48–7.36 (m,  
619 2H), 4.36 (t,  $J$  = 6.8 Hz, 2H), 2.64 (t,  $J$  = 6.8 Hz, 2H), 2.12 (qn,  $J$  = 6.8  
620 Hz, 2H).

621 **4,4-Difluorobutyl benzoate (1c)**. To a stirred solution of **1b** (11  
622 mmol, 2.1 g) in dry CH<sub>2</sub>Cl<sub>2</sub> (20 mL), (diethylamino)sulfur trifluoride  
623 (DAST; 20 mmol, 2.6 mL) was added dropwise at 0 °C via syringe  
624 under N<sub>2</sub> atmosphere. After 10 min, the reaction mixture was allowed to  
625 warm to room temperature and stirred for additional 50 min. The  
626 reaction mixture was then cooled to 0 °C and carefully quenched with  
627 20 mL of saturated NaHCO<sub>3</sub>. The mixture was then extracted with  
628 CH<sub>2</sub>Cl<sub>2</sub> (3  $\times$  40 mL). The collected organic layers were dried over  
629 anhydrous Na<sub>2</sub>SO<sub>4</sub> and concentrated under rotary evaporation. The

crude residue was purified by column chromatography (eluent: ethyl  
acetate in *n*-hexane, 0.5%). Yield: 40%. <sup>1</sup>H NMR (300 MHz, CDCl<sub>3</sub>)  $\delta$ :  
631 8.09–7.98 (m, 2H), 7.61–7.51 (m, 1H), 7.49–7.39 (m, 2H), 5.90 (tt,  $J$   
632 = 56.5, 4.0 Hz, 1H), 4.37 (t,  $J$  = 6.0 Hz, 2H), 2.20–1.83 (m, 4H). 633

**4,4-Difluorobutyl 4-Nitrobenzenesulfonate (1d)**. By applying  
634 slight modifications to a reported procedure,<sup>41</sup> sodium methoxide  
635 powder (4.8 mmol, 0.26 g) was added in one portion to a stirred  
636 solution of **1c** (3.2 mmol, 0.68 g) in MeOH (10 mL) cooled to 0 °C.  
637 After 1.5 h at room temperature, trifluoroacetic acid (4.8 mmol, 0.37  
638 mL) was added while cooling to 0 °C and the clear mixture was stirred  
639 for 30 min at room temperature. Methanol was then removed under  
640 rotary evaporation and the residue partitioned between Et<sub>2</sub>O (20 mL)  
641 and brine (40 mL). The aqueous layer was extracted with Et<sub>2</sub>O (3  $\times$  20  
642 mL), then the organic phases were collected and concentrated to  
643 dryness. The crude product was dissolved in dry CH<sub>2</sub>Cl<sub>2</sub> (20 mL)  
644 followed by the addition of Et<sub>3</sub>N (4.8 mmol, 0.66 mL), 4-  
645 nitrobenzenesulfonyl chloride (3.8 mmol, 0.84 g), and 4-  
646 (dimethylamino)pyridine (DMAP; 0.32 mmol, 0.040 g). The reaction  
647 mixture was stirred at room temperature for 1.5 h, then quenched with  
648 saturated NH<sub>4</sub>Cl (40 mL), and extracted with ethyl acetate (3  $\times$  30  
649 mL). The collected organic layers were dried over Na<sub>2</sub>SO<sub>4</sub> and  
650 concentrated under reduced pressure. The resulting crude was purified  
651 by column chromatography (gradient eluent: ethyl acetate in *n*-hexane,  
652 0  $\rightarrow$  20%) to afford difluoride **1d** as a yellow oil. Yield: 38%. <sup>1</sup>H NMR  
653 (500 MHz, CDCl<sub>3</sub>)  $\delta$ : 8.44–8.39 (m, 2H), 8.14–8.07 (m, 2H), 5.84  
654 (tt,  $J$  = 56.3, 3.6 Hz, 1H), 4.21 (t,  $J$  = 5.9 Hz, 2H), 2.01–1.82 (m, 4H). 655

**General Procedures for N-Alkylation Reactions.** Method A:  
656 Piperidine intermediate **2b**<sup>33</sup> (0.34 mmol, 0.10 g) was suspended in  
657 acetonitrile (1.5 mL) before adding anhydrous K<sub>2</sub>CO<sub>3</sub> (0.68 mmol,  
658 0.096 g) and the suitable benzyl bromide (0.34 mmol). The reaction  
659 was refluxed for 5 h, and the solvent was evaporated under reduced  
660 pressure. The resulting crude was suspended in CH<sub>2</sub>Cl<sub>2</sub>, and the  
661 inorganic solid residue was filtered off after thorough washing. The  
662 solvent was removed under rotary evaporation, and the desired  
663 products were isolated as described below. 664

Method B: To a solution of appropriate amine (30 mmol) in THF (6  
665 mL), aliquots (0.4 mL) of 3-fluorobenzylbromide (1.5–3.0 mmol)  
666 previously dissolved in THF (3.0 mL) were added at every 45 min  
667 interval (after TLC monitoring to check bromide consumption). The  
668 excess amine was evaporated, then the reaction mixture was diluted  
669 with brine (20 mL), and extracted with CH<sub>2</sub>Cl<sub>2</sub> (3  $\times$  10 mL). The  
670 collected organic layers were dried over anhydrous Na<sub>2</sub>SO<sub>4</sub>,  
671 concentrated under rotary evaporation, and purified by flash  
672 chromatography (gradient: methanol in dichloromethane, 0  $\rightarrow$  10%). 673

Method C: Intermediate **9a**<sup>57</sup> (0.20 mmol, 0.062 g) was solubilized  
674 in acetonitrile (4 mL). K<sub>2</sub>CO<sub>3</sub> (0.40 mmol, 0.055 g), appropriate amine  
675 (0.40 mmol), and a catalytic amount of KI were added. The reaction  
676 mixture was refluxed under magnetic stirring for 10 h. After cooling to  
677 room temperature, the mixture was concentrated to dryness, and the  
678 residue was suspended with CH<sub>2</sub>Cl<sub>2</sub>. The inorganic solid was filtered off  
679 and washed with CH<sub>2</sub>Cl<sub>2</sub>. The solvent was removed under rotatory  
680 evaporation, and the resulting crude was purified through flash  
681 chromatography (gradient: methanol in dichloromethane, 0  $\rightarrow$  5%). 682

Method D: Appropriate derivatives **9b**,<sup>34</sup> **9c-d**<sup>18</sup> (0.50 mmol) were  
683 dissolved in THF (1.6 mL). Aliquots (0.2 mL) of this solution were  
684 added at 45 min intervals under N<sub>2</sub> atmosphere to a round-bottom flask  
685 containing commercially available 2.0 M CH<sub>3</sub>NH<sub>2</sub> solution in THF  
686 (5.0 mL). Once additions were complete, the reaction mixture was left  
687 at room temperature under magnetic stirring overnight. The excess  
688 methylamine and THF were evaporated to dryness. The resulting crude  
689 was purified as described below. 690

Method E: The appropriate intermediate **2a-b**<sup>33</sup> or **12a-c** (0.24  
691 mmol) was dissolved in acetonitrile (1 mL) followed by the addition of  
692 K<sub>2</sub>CO<sub>3</sub> (0.24 mmol, 0.033 g). Intermediate **1d** (0.22 mmol, 0.065 g) or  
693 commercially available 3-bromo-1-propanol (0.22 mmol, 20  $\mu$ L) was  
694 then added to this mixture. The vessel was sealed, and the resulting  
695 reaction mixture was left under magnetic stirring at 80 °C for 4–18 h.  
696 After cooling to room temperature, the reaction was concentrated to  
697 dryness. The solid residue was dissolved in CHCl<sub>3</sub> and the inorganic  
698

699 residue was filtered off. The solution was concentrated under reduced  
700 pressure, and the resulting crude was purified as described below.

701 7-[[1-(4,4-Difluorobutyl)piperidin-3-yl]methoxy]-3,4-dimethyl-  
702 2H-chromen-2-one ((±)-**4**). Method E: prepared from **2a** (0.24 mmol,  
703 0.069 g) and **1d** (0.22 mmol, 0.065 g). Purification procedure: column  
704 chromatography (gradient eluent: methanol in CH<sub>2</sub>Cl<sub>2</sub>, 0 → 2%).  
705 Yield: 51%; white solid; mp: 74–76 °C. <sup>1</sup>H NMR (300 MHz, CDCl<sub>3</sub>)  
706 δ: 7.48 (d, *J* = 8.8 Hz, 1H), 6.84 (dd, *J* = 8.8, 2.4 Hz, 1H), 6.78 (d, *J* = 2.4  
707 Hz, 1H), 5.86 (tt, *J* = 56.7, 4.3 Hz, 1H), 3.93–3.82 (m, 2H), 3.06–2.93  
708 (m, 1H), 2.90–2.76 (m, 1H), 2.46–2.38 (m, 2H), 2.37 (s, 3H), 2.18 (s,  
709 3H), 2.09–1.88 (m, 2H), 1.87–1.76 (m, 2H), 1.76–1.67 (m, 3H),  
710 1.67–1.52 (m, 4H). <sup>13</sup>C NMR (126 MHz, CDCl<sub>3</sub>) δ: 162.48 (s),  
711 160.97 (s), 153.52 (s), 146.25 (s), 125.18 (s), 118.85 (s), 117.30 (t, *J* =  
712 238.7 Hz), 114.09 (s), 112.43 (s), 101.03 (s), 71.32 (s), 58.02 (s),  
713 57.01 (s), 54.04 (s), 36.07 (s), 32.13 (t, *J* = 21.0 Hz), 27.24 (s), 24.67  
714 (s), 19.51 (t, *J* = 5.3 Hz), 15.09 (s), 13.15 (s). Anal. (C<sub>21</sub>H<sub>27</sub>F<sub>2</sub>NO<sub>3</sub>)  
715 calcd % C, 66.47; H, 7.17; N, 3.69; found % C, 66.90; H, 6.91; N, 3.81.  
716 HRMS (Q-TOF) calcd for (C<sub>21</sub>H<sub>27</sub>F<sub>2</sub>NO<sub>3</sub>): [M + H]<sup>+</sup> *m/z*: 380.2032,  
717 found 380.2046; [M + Na]<sup>+</sup> *m/z*: 402.1851, found 402.1864.

718 7-[[1-(3-Fluorobenzyl)piperidin-4-yl]methoxy]-3,4-dimethyl-2H-  
719 chromen-2-one (**5**). Method A: prepared from 3-fluorobenzylbromide  
720 (0.34 mmol, 0.042 mL). Purification procedure: column chromatog-  
721 raphy (eluent: ethyl acetate in CH<sub>2</sub>Cl<sub>2</sub>, 50%). Yield: 64%; white solid;  
722 mp: 123–126 °C. <sup>1</sup>H NMR (300 MHz, CDCl<sub>3</sub>) δ: 7.48 (d, *J* = 8.8 Hz,  
723 1H), 7.32–7.21 (m, 1H), 7.13–7.02 (m, 2H), 6.99–6.90 (m, 1H), 6.83  
724 (dd, *J* = 8.8, 2.5 Hz, 1H), 6.78 (d, *J* = 2.5 Hz, 1H), 3.85 (d, *J* = 5.8 Hz,  
725 2H), 3.51 (s, 2H), 2.99–2.86 (m, 2H), 2.37 (s, 3H), 2.18 (s, 3H),  
726 2.09–1.93 (m, 2H), 1.88–1.73 (m, 3H), 1.53–1.35 (m, 2H). <sup>13</sup>C NMR  
727 (126 MHz, DMSO-*d*<sub>6</sub>) δ: 158.16 (d, *J* = 245.3 Hz), 157.67 (s), 156.27  
728 (s), 148.78 (s), 141.45 (s), 136.57 (d, *J* = 5.0 Hz), 124.79 (d, *J* = 8.2  
729 Hz), 120.42 (s), 119.72 (d, *J* = 2.7 Hz), 114.08 (s), 110.93 (d, *J* = 21.3  
730 Hz), 109.32 (s), 109.04 (d, *J* = 21.2 Hz), 107.58 (s), 96.35 (s), 68.24  
731 (s), 58.00 (d, *J* = 1.4 Hz), 48.53 (s), 30.94 (s), 24.20 (s), 10.33 (s), 8.43  
732 (s). Anal. (C<sub>24</sub>H<sub>26</sub>FNO<sub>3</sub>) calcd % C, 72.89; H, 6.63; N, 3.54; found %  
733 C, 73.12; H, 6.50; N, 3.59. HRMS (Q-TOF) calcd for (C<sub>24</sub>H<sub>26</sub>FNO<sub>3</sub>):  
734 [M + H]<sup>+</sup> *m/z*: 396.1969, found 396.1979; [M + Na]<sup>+</sup> *m/z*: 418.1789,  
735 found 418.1807.

736 3,4-Dimethyl-7-((1-[3-(trifluoromethyl)benzyl]piperidin-4-yl)-  
737 methoxy)-2H-chromen-2-one (**6**). Method A: prepared from 3-  
738 (trifluoromethyl)benzyl bromide (0.34 mmol, 0.052 mL). Purification  
739 procedure: flash chromatography (gradient eluent: ethyl acetate in  
740 CH<sub>2</sub>Cl<sub>2</sub>, 0 → 30%). Yield: 80%; white solid; mp: 113–115 °C. <sup>1</sup>H  
741 NMR (500 MHz, DMSO-*d*<sub>6</sub>) δ: 7.66 (d, *J* = 9.6 Hz, 1H), 7.63–7.57 (m,  
742 3H), 7.57–7.52 (m, 1H), 6.95–6.88 (m, 2H), 3.92 (d, *J* = 5.9 Hz, 2H),  
743 3.54 (s, 2H), 2.88–2.74 (m, 2H), 2.34 (s, 3H), 2.05 (s, 3H), 2.02–1.90  
744 (m, 2H), 1.79–1.67 (m, 3H), 1.38–1.22 (m, 2H). <sup>13</sup>C NMR (126  
745 MHz, DMSO-*d*<sub>6</sub>) δ: 157.67 (s), 156.24 (s), 148.78 (s), 141.44 (s),  
746 134.84 (s), 127.58 (s), 125.79 (q, *J* = 31.9 Hz), 123.89 (s), 120.85 (s),  
747 120.54 (q, *J* = 272.2 Hz), 120.43 (s), 119.12 (s), 114.10 (s), 109.35 (s),  
748 107.57 (s), 96.36 (s), 68.17 (s), 57.96 (s), 48.52 (s), 30.89 (s), 24.15  
749 (s), 10.29 (s), 8.38 (s). Anal. (C<sub>25</sub>H<sub>26</sub>F<sub>3</sub>NO<sub>3</sub>) calcd % C, 67.40; H,  
750 5.88; N, 3.14; found % C, 67.84; H, 6.01; N, 3.03. HRMS (Q-TOF)  
751 calcd for (C<sub>25</sub>H<sub>26</sub>F<sub>3</sub>NO<sub>3</sub>): [M + H]<sup>+</sup> *m/z*: 446.1938, found 446.1945;  
752 [M + Na]<sup>+</sup> *m/z*: 468.1757, found 468.1770.

753 7-[[1-(4,4-Difluorobutyl)piperidin-4-yl]methoxy]-3,4-dimethyl-  
754 2H-chromen-2-one (**7**). Method E: prepared from **2b** (0.24 mmol,  
755 0.069 g) and **1d** (0.22 mmol, 0.065 g). Purification procedure: column  
756 chromatography (gradient eluent: methanol in CH<sub>2</sub>Cl<sub>2</sub>, 0 → 2%).  
757 Yield: 46%; pale yellow solid; mp: 102–104 °C. <sup>1</sup>H NMR (500 MHz,  
758 CDCl<sub>3</sub>) δ: 7.48 (d, *J* = 8.9 Hz, 1H), 6.83 (dd, *J* = 8.9, 2.5 Hz, 1H), 6.78  
759 (d, *J* = 2.5 Hz, 1H), 5.86 (tt, *J* = 57.0, 4.4 Hz, 1H), 3.85 (d, *J* = 5.9 Hz,  
760 2H), 2.96 (d, *J* = 11.2 Hz, 2H), 2.39 (t, *J* = 7.4 Hz, 2H), 2.36 (s, 3H),  
761 2.18 (s, 3H), 1.98 (t, *J* = 11.3 Hz, 2H), 1.92–1.78 (m, 5H), 1.67 (qn, *J* =  
762 7.4 Hz, 2H), 1.51–1.36 (m, 2H). <sup>13</sup>C NMR (126 MHz, CDCl<sub>3</sub>) δ:  
763 162.40 (s), 160.91 (s), 153.52 (s), 146.17 (s), 125.21 (s), 118.90 (s),  
764 117.12 (t, *J* = 237.5 Hz), 114.15 (s), 112.25 (s), 101.15 (s), 72.75 (s),  
765 57.76 (s), 53.19 (s), 35.60 (s), 32.07 (t, *J* = 21.4 Hz), 28.65 (s), 19.32  
766 (s), 15.05 (s), 13.13 (s). Anal. (C<sub>21</sub>H<sub>27</sub>F<sub>2</sub>NO<sub>3</sub>) calcd % C, 66.47; H,  
767 7.17; N, 3.69; found % C, 66.71; H, 7.02; N, 3.77. HRMS (Q-TOF)

calcd for (C<sub>21</sub>H<sub>27</sub>F<sub>2</sub>NO<sub>3</sub>): [M + H]<sup>+</sup> *m/z*: 380.2032, found 380.2037; 768  
[M + Na]<sup>+</sup> *m/z*: 402.1851, found 402.1851. 769

770 1-(3-Fluorophenyl)-N-methylmethanamine Hydrochloride (**8a**). 770  
Method B: prepared from 2.0 N methylamine in THF (30 mmol, 15 771  
mL) and 3-fluorobenzylbromide (3.0 mmol, 0.40 mL). The compound 772  
was transformed into the corresponding hydrochloride salt by 773  
dissolving the solid free base in the minimum volume of 1,4-dioxane 774  
before adding 4.0 N HCl in 1,4-dioxane. The resulting precipitate was 775  
collected by filtration and washed with dry dioxane, yielding **8a**. Yield: 776  
49%. <sup>1</sup>H NMR (500 MHz, DMSO-*d*<sub>6</sub>) δ: 9.08 (br s, 2H), 7.51–7.47 777  
(m, 1H), 7.40–7.38 (m, 1H), 7.35–7.33 (m, 1H), 7.28–7.24 (m, 1H), 778  
4.13 (s, 2H), 2.53 (s, 3H). 779

780 N-(3-Fluorobenzyl)ethanamine (**8b**). Method B: prepared from aq. 780  
66% w/v ethylamine (30 mmol, 2.0 mL) and 3-fluorobenzylbromide 781  
(1.5 mmol, 0.18 mL). Yield: 53%. <sup>1</sup>H NMR (300 MHz, DMSO-*d*<sub>6</sub>) δ: 782  
7.43–7.26 (m, 1H), 7.19–7.06 (m, 2H), 7.06–6.91 (m, 1H), 3.66 (s, 783  
2H), 2.47 (q, *J* = 7.1 Hz, 2H), 0.99 (t, *J* = 7.1 Hz, 3H), NH not detected. 784

785 N-(3-Fluorobenzyl)propan-2-amine (**8c**). Method B: prepared 785  
from isopropylamine (30 mmol, 2.6 mL) and 3-fluorobenzylbromide 786  
(1.5 mmol, 0.18 mL). Yield: 42%. <sup>1</sup>H NMR (300 MHz, DMSO-*d*<sub>6</sub>) δ: 787  
7.37–7.23 (m, 1H), 7.19–7.09 (m, 2H), 7.06–6.91 (m, 1H), 3.67 (s, 788  
2H), 2.65 (h, *J* = 6.2 Hz, 1H), 1.96 (s, 1H), 0.96 (d, *J* = 6.2 Hz, 6H). 789

790 7-[3-[Ethyl(3-fluorobenzyl)amino]propoxy]-3,4-dimethyl-2H-  
791 chromen-2-one (**10**). Method C: prepared from **8b** (0.40 mmol, 0.060 791  
g). Yield: 80%; yellow solid; mp: 65–67 °C. <sup>1</sup>H NMR (300 MHz, 792  
DMSO-*d*<sub>6</sub>) δ: 7.65 (d, *J* = 9.1 Hz, 1H), 7.33–7.23 (m, 1H), 7.15–7.04 793  
7.43–7.26 (m, 1H), 7.19–7.06 (m, 1H), 6.89–6.81 (m, 2H), 4.06 (t, *J* = 6.4 Hz, 794  
2H), 3.54 (s, 2H), 2.53 (d, *J* = 6.4 Hz, 2H), 2.44 (q, *J* = 7.1 Hz, 2H), 795  
2.35 (s, 3H), 2.06 (s, 3H), 1.85 (qn, *J* = 6.4 Hz, 2H), 0.96 (t, *J* = 7.1 Hz, 796  
3H). <sup>13</sup>C NMR (126 MHz, CDCl<sub>3</sub>) δ: 162.89 (d, *J* = 245.5 Hz), 162.46 797  
(s), 160.92 (s), 153.52 (s), 146.22 (s), 142.55 (s), 129.55 (s), 125.15 798  
(s), 124.07 (s), 118.81 (s), 115.34 (d, *J* = 20.0 Hz), 114.07 (s), 113.59 799  
(d, *J* = 20.0 Hz), 112.24 (s), 101.14 (s), 66.35 (s), 57.78 (s), 49.39 (s), 800  
47.51 (s), 26.87 (s), 15.05 (s), 13.13 (s), 11.88 (s). Anal. 801  
(C<sub>23</sub>H<sub>26</sub>FNO<sub>3</sub>) calcd % C, 72.04; H, 6.83; N, 3.65; found % C, 802  
71.86; H, 6.63; N, 3.74. HRMS (Q-TOF) calcd for (C<sub>23</sub>H<sub>26</sub>FNO<sub>3</sub>): [M 803  
+ H]<sup>+</sup> *m/z*: 384.1969, found 384.1980; [M + Na]<sup>+</sup> *m/z*: 406.1789, 804  
found 406.1806. 805

806 7-[[3-(3-Fluorobenzyl)(isopropyl)amino]propoxy]-3,4-dimethyl-  
807 2H-chromen-2-one (**11**). Method C: prepared from **8c** (0.40 mmol, 807  
0.067 g). Yield: 30%; white solid; mp: 101–102 °C. <sup>1</sup>H NMR (300 808  
MHz, DMSO-*d*<sub>6</sub>) δ: 7.65 (d, *J* = 9.5 Hz, 1H), 7.32–7.22 (m, 1H), 809  
7.16–7.05 (m, 2H), 6.99–6.90 (m, 1H), 6.87–6.79 (m, 2H), 4.04 (t, *J* 810  
= 6.3 Hz, 2H), 3.54 (s, 2H), 2.83 (heptet, *J* = 6.5 Hz, 1H), 2.54 (t, *J* = 811  
6.3 Hz, 2H), 2.35 (s, 3H), 2.06 (s, 3H), 1.77 (qn, *J* = 6.3 Hz, 2H), 0.95 812  
(d, *J* = 6.5 Hz, 6H). <sup>13</sup>C NMR (126 MHz, CDCl<sub>3</sub>) δ: 162.93 (d, *J* = 813  
244.6 Hz), 162.49 (s), 161.01 (s), 153.52 (s), 146.25 (s), 144.17 (d, *J* = 814  
6.9 Hz), 129.46 (d, *J* = 8.2 Hz), 125.10 (s), 123.70 (d, *J* = 2.4 Hz), 815  
118.72 (s), 114.96 (d, *J* = 21.3 Hz), 113.98 (s), 113.38 (d, *J* = 21.4 Hz), 816  
112.26 (s), 101.09 (s), 66.24 (s), 53.74 (s), 49.73 (s), 45.55 (s), 27.94 817  
(s), 17.82 (s), 15.04 (s), 13.12 (s). Anal. (C<sub>24</sub>H<sub>28</sub>FNO<sub>3</sub>) calcd % C, 818  
72.52; H, 7.10; N, 3.52; found % C, 72.13; H, 6.96; N, 3.52. HRMS (Q- 819  
TOF) calcd for (C<sub>24</sub>H<sub>28</sub>FNO<sub>3</sub>): [M + H]<sup>+</sup> *m/z*: 398.2126, found 820  
398.2134; [M + Na]<sup>+</sup> *m/z*: 420.1945, found 420.1959. 821

822 4-(Hydroxymethyl)-7-((4-[(methylamino)methyl]benzyl)oxy)-2H-  
823 chromen-2-one (**12a**). Method D: prepared from **9b** (0.50 mmol, 0.19 823  
g). Purification procedure: column chromatography (gradient eluent: 824  
methanol in CH<sub>2</sub>Cl<sub>2</sub>, 10 → 20%). Yield: 75%; yellow solid. <sup>1</sup>H NMR 825  
(300 MHz, DMSO-*d*<sub>6</sub>) δ: 7.61 (d, *J* = 8.8 Hz, 1H), 7.53 (d, *J* = 8.3 Hz, 826  
2H), 7.49 (d, *J* = 8.3 Hz, 2H), 7.06 (d, *J* = 2.4 Hz, 1H), 6.99 (dd, *J* = 8.8, 827  
2.4 Hz, 1H), 6.29 (s, 1H), 5.61 (t, *J* = 5.5 Hz, 1H), 5.25 (s, 2H), 4.71 (d, 828  
*J* = 5.5 Hz, 2H), 4.11 (s, 2H), 2.54 (s, 3H), NH not detected. 829

830 3,4-Dimethyl-7-[[3-[(methylamino)methyl]benzyl]oxy]-2H-chro-  
831 men-2-one (**12b**). Method D: prepared from **9c** (0.50 mmol, 0.16 g). 831  
Purification procedure: column chromatography (gradient eluent: 832  
methanol in CH<sub>2</sub>Cl<sub>2</sub>, 10 → 20%). Yield: 88%; pale yellow solid. <sup>1</sup>H 833  
NMR (300 MHz, DMSO-*d*<sub>6</sub>) δ: 7.70 (d, *J* = 8.6 Hz, 1H), 7.59 (s, 1H), 834  
7.54–7.36 (m, 3H), 7.10–6.91 (m, 2H), 5.20 (s, 2H), 4.06 (s, 2H), 835  
2.50 (s, 3H), 2.35 (s, 3H), 2.09 (s, 3H), NH not detected. 836

837 **3,4-Dimethyl-7-((4-((methylamino)methyl)benzyl)oxy)-2H-chro-**  
838 **men-2-one (12c).** Method D: prepared from **9d** (0.50 mmol, 0.19 g).  
839 Purified through washing several times the crude solid with Et<sub>2</sub>O (3.5  
840 mL) and a mixture of Et<sub>2</sub>O/*n*-hexane (4.5/0.5 v/v) until disappearance  
841 of impurities in TLC control. Yield: 93%; white solid. <sup>1</sup>H NMR (300  
842 MHz, DMSO-*d*<sub>6</sub>) δ: 7.69 (d, *J* = 9.1 Hz, 1H), 7.47 (d, *J* = 8.2 Hz, 2H),  
843 7.42 (d, *J* = 8.2 Hz, 2H), 7.05–6.95 (m, 2H), 5.20 (s, 2H), 3.90 (s, 2H),  
844 2.41 (s, 3H), 2.36 (s, 3H), 2.35 (s, 3H), NH not detected.  
845 **7-((3-((4,4-Difluorobutyl)(methylamino)methyl)benzyl)oxy)-**  
846 **3,4-dimethyl-2H-chromen-2-one (13).** Method E: prepared from **12b**  
847 (0.24 mmol, 0.079 g) and **1d** (0.22 mmol, 0.065 g). Purification  
848 procedure: column chromatography (gradient eluent: methanol in  
849 CH<sub>2</sub>Cl<sub>2</sub>, 1 → 2%). Yield: 42%; off-white solid; mp: 73–75 °C. <sup>1</sup>H NMR  
850 (500 MHz, CDCl<sub>3</sub>) δ: 7.50 (d, *J* = 8.9 Hz, 1H), 7.40 (s, 1H), 7.38–7.28  
851 (m, 3H), 6.92 (dd, *J* = 8.9, 2.5 Hz, 1H), 6.86 (d, *J* = 2.5 Hz, 1H), 5.83  
852 (tt, *J* = 57.0, 4.4 Hz, 1H), 5.11 (s, 2H), 3.55 (s, 2H), 2.44 (t, *J* = 6.3 Hz,  
853 2H), 2.36 (s, 3H), 2.22 (s, 3H), 2.18 (s, 3H), 1.93–1.81 (m, 2H),  
854 1.73–1.64 (m, 2H). <sup>13</sup>C NMR (126 MHz, CDCl<sub>3</sub>) δ: 162.41 (s),  
855 160.53 (s), 153.43 (s), 146.24 (s), 139.12 (s), 136.11 (s), 128.98 (s),  
856 128.73 (s), 128.09 (s), 126.41 (s), 125.29 (s), 119.03 (s), 117.26 (t, *J* =  
857 238.7 Hz), 114.36 (s), 112.73 (s), 101.58 (s), 70.31 (s), 62.03 (s),  
858 56.17 (s), 41.84 (s), 31.82 (t, *J* = 21.0 Hz), 19.73 (s), 15.08 (s), 13.16  
859 (s). Anal. (C<sub>24</sub>H<sub>27</sub>F<sub>2</sub>NO<sub>3</sub>) calcd % C, 69.38; H, 6.55; N, 3.37; found %  
860 C, 69.54; H, 6.61; N, 3.32. HRMS (Q-TOF) calcd for (C<sub>24</sub>H<sub>27</sub>F<sub>2</sub>NO<sub>3</sub>):  
861 [M + H]<sup>+</sup> *m/z*: 416.2032, found 416.2040; [M + Na]<sup>+</sup> *m/z*: 438.1851,  
862 found 438.1862.  
863 **7-((4-((4,4-Difluorobutyl)(methylamino)methyl)benzyl)oxy)-**  
864 **3,4-dimethyl-2H-chromen-2-one (14).** Method E: prepared from **12c**  
865 (0.24 mmol, 0.79 g) and **1d** (0.22 mmol, 0.065 g). Purification  
866 procedure: column chromatography (gradient eluent: methanol in  
867 CH<sub>2</sub>Cl<sub>2</sub>, 1 → 2%). Yield: 45%; off-white solid; mp: 67–69 °C. <sup>1</sup>H NMR  
868 (300 MHz, CDCl<sub>3</sub>) δ: 7.50 (d, *J* = 8.8 Hz, 1H), 7.39 (d, *J* = 8.1 Hz, 2H),  
869 7.34 (d, *J* = 8.1 Hz, 2H), 6.92 (dd, *J* = 8.8, 2.5 Hz, 1H), 6.87 (d, *J* = 2.5  
870 Hz, 1H), 5.83 (tt, *J* = 56.9, 4.3 Hz, 1H), 5.10 (s, 2H), 3.52 (s, 2H), 2.43  
871 (br s, 2H), 2.37 (s, 3H), 2.21 (s, 3H), 2.18 (s, 3H), 2.00–1.74 (m, 2H),  
872 1.76–1.62 (m, 2H). <sup>13</sup>C NMR (126 MHz, CDCl<sub>3</sub>) δ: 162.38 (s),  
873 160.52 (s), 153.46 (s), 146.17 (s), 135.19 (s), 129.50 (s), 127.83 (s),  
874 127.76 (s), 125.27 (s), 119.07 (s), 117.15 (t, *J* = 239.2 Hz), 114.39 (s),  
875 112.71 (s), 101.61 (s), 70.14 (s), 61.67 (s), 56.05 (s), 41.57 (s), 31.77  
876 (t, *J* = 21.0 Hz), 19.56 (s), 15.05 (s), 13.13 (s). Anal. (C<sub>24</sub>H<sub>27</sub>F<sub>2</sub>NO<sub>3</sub>)  
877 calcd % C, 69.38; H, 6.55; N, 3.37; found % C, 69.70; H, 6.48; N, 3.41.  
878 HRMS (Q-TOF) calcd for (C<sub>24</sub>H<sub>27</sub>F<sub>2</sub>NO<sub>3</sub>): [M + H]<sup>+</sup> *m/z*: 416.2032,  
879 found 416.2030; [M + Na]<sup>+</sup> *m/z*: 438.1851, found 438.1851.  
880 **7-((4-((4,4-Difluorobutyl)(methylamino)methyl)benzyl)oxy)-4-**  
881 **(hydroxymethyl)-2H-chromen-2-one (15).** Method E: prepared from  
882 **12a** (0.24 mmol, 0.076 g) and **1d** (0.22 mmol, 0.065 g). Purification  
883 procedure: column chromatography (gradient eluent: methanol in  
884 CH<sub>2</sub>Cl<sub>2</sub>, 1 → 5%). Yield: 50%; glass solid. <sup>1</sup>H NMR (300 MHz, CDCl<sub>3</sub>)  
885 δ: 7.42 (d, *J* = 9.2 Hz, 1H), 7.38 (d, *J* = 8.3 Hz, 2H), 7.33 (d, *J* = 8.3 Hz,  
886 2H), 6.98–6.86 (m, 2H), 6.46 (s, 1H), 5.83 (tt, *J* = 57.0, 4.4 Hz, 1H),  
887 5.11 (s, 2H), 4.87 (s, 2H), 3.51 (s, 2H), 2.42 (t, *J* = 7.0 Hz, 2H), 2.20 (s,  
888 3H), 2.03–1.44 (m, 4H), OH not detected. <sup>13</sup>C NMR (126 MHz,  
889 CDCl<sub>3</sub>) δ: 161.64 (s), 161.58 (s), 155.24 (s), 154.52 (s), 137.60 (s),  
890 135.01 (s), 129.62 (s), 127.62 (s, *J* = 34.5 Hz), 124.43 (s), 117.13 (t, *J* =  
891 238.9 Hz), 113.11 (s), 111.14 (s), 108.87 (s), 102.02 (s), 70.17 (s),  
892 61.63 (s), 60.68 (s), 56.08 (s), 41.59 (s), 31.75 (t, *J* = 21.1 Hz), 19.44  
893 (s). Anal. (C<sub>23</sub>H<sub>25</sub>F<sub>2</sub>NO<sub>4</sub>) calcd % C, 66.18; H, 6.04; N, 3.36; found %  
894 C, 66.32; H, 5.97; N, 3.30. HRMS (Q-TOF) calcd for (C<sub>23</sub>H<sub>25</sub>F<sub>2</sub>NO<sub>4</sub>):  
895 [M + H]<sup>+</sup> *m/z*: 418.1824, found 418.1824; [M + Na]<sup>+</sup> *m/z*: 440.1644,  
896 found 440.1645.  
897 **7-((4-((3-Fluorobenzyl)(methylamino)methyl)benzyl)oxy)-4-**  
898 **(hydroxymethyl)-2H-chromen-2-one hydrochloride (16).** In a pyrex  
899 vessel charged with a magnetic stirring bar, intermediate **9b** (0.40  
900 mmol, 0.15 g) was suspended in acetone (10 mL), followed by the  
901 addition of K<sub>2</sub>CO<sub>3</sub> (1.6 mmol, 0.220 g), **8a** (0.80 mmol, 0.11 g), and a  
902 catalytic amount of KI. The reaction was kept under microwave  
903 irradiation for 30 min at 130 °C. After cooling to room temperature, the  
904 solid residue was filtered-off and thoroughly washed with CHCl<sub>3</sub>. The  
905 resulting solution was concentrated under reduced pressure and  
906 purified by flash chromatography (gradient eluent: methanol in

CH<sub>2</sub>Cl<sub>2</sub>, 0 → 10%). The compound was transformed into the 907  
corresponding hydrochloride salt by dissolving the solid free base in the 908  
minimum volume of 1,4-dioxane before adding HCl 4.0 N in 1,4- 909  
dioxane. The resulting precipitate was collected by filtration and 910  
washed with dry dioxane, thus obtaining **16**. Yield: 61%; white solid; 911  
mp: >230 °C. <sup>1</sup>H NMR (500 MHz, DMSO-*d*<sub>6</sub>) δ: 10.37 (s, 1H, dis. 912  
with D<sub>2</sub>O), 7.63 (d, *J* = 8.8 Hz, 1H), 7.60 (d, *J* = 8.2 Hz, 2H), 7.57 (d, *J* = 913  
8.2 Hz, 2H), 7.55–7.45 (m, 2H), 7.42–7.38 (m, 1H), 7.35–7.28 (m, 914  
1H), 7.10 (d, *J* = 2.5 Hz, 1H), 7.02 (dd, *J* = 8.8, 2.5 Hz, 1H), 6.30 (s, 915  
1H), 5.63 (s, 1H), 5.27 (s, 2H), 4.72 (s, 2H), 4.54–4.36 (m, 2H), 916  
4.30–4.11 (m, 2H), 2.53 (d, *J* = 4.8 Hz, 3H). <sup>13</sup>C NMR (126 MHz, 917  
DMSO-*d*<sub>6</sub>) δ: 162.34 (d, *J* = 244.4 Hz), 161.51 (s), 160.86 (s), 157.14 918  
(s), 155.11 (s), 138.12 (s), 133.00 (d, *J* = 7.9 Hz), 132.15 (s), 131.25 (d, 919  
*J* = 8.3 Hz), 130.07 (s), 128.50 (s), 128.08 (d, *J* = 2.5 Hz), 125.91 (s), 920  
118.66 (d, *J* = 22.2 Hz), 116.89 (d, *J* = 20.8 Hz), 113.09 (s), 111.37 (s), 921  
108.01 (s), 102.20 (s), 69.75 (s), 66.78 (s), 59.49 (s), 58.39 (s), 57.94 922  
(s). Anal. (C<sub>26</sub>H<sub>25</sub>ClFNO<sub>4</sub>) calcd % C, 66.45; H, 5.36; N, 2.98; found % 923  
C, 66.63; H, 5.59; N, 3.11. HRMS (Q-TOF) calcd for (C<sub>26</sub>H<sub>24</sub>ClFNO<sub>4</sub>): 924  
[M + H]<sup>+</sup> *m/z*: 434.1762, found 434.1772; [M + Na]<sup>+</sup> *m/z*: 456.1582, 925  
found 456.1594; [M – H]<sup>–</sup> *m/z*: 432.1617, found 432.1602. 926

**7-((4-((Benzyl(methylamino)methyl)benzyl)oxy)-2-oxo-2H-chro-** 927  
**mene-4-carbaldehyde (18).** In a flame-dried round-bottom flask, **17**<sup>34</sup> 928  
(0.51 mmol, 0.21 g) was dissolved in anhydrous CH<sub>2</sub>Cl<sub>2</sub> (10 mL). 929  
MnO<sub>2</sub> powder (10 mmol, 0.90 g) was added to the solution, and the 930  
reaction mixture was stirred at room temperature for 2 h. After this 931  
period, the mixture was diluted with Et<sub>2</sub>O (75 mL), the inorganic 932  
residue was filtered off through a pad of silica gel and carefully washed 933  
with Et<sub>2</sub>O. The resulting solution was then concentrated under rotary 934  
evaporation affording the desired aldehyde. Yield: 64%; yellow solid. <sup>1</sup>H 935  
NMR (300 MHz, CDCl<sub>3</sub>) δ: 10.06 (s, 1H), 8.49 (d, *J* = 9.0 Hz, 1H), 936  
7.46–7.37 (m, 5H), 7.36–7.28 (m, 4H), 6.99 (dd, *J* = 9.0, 2.5 Hz, 1H), 937  
6.93 (d, *J* = 2.5 Hz, 1H), 6.70 (s, 1H), 5.13 (s, 2H), 3.53 (s, 4H), 2.19 (s, 938  
3H). 939

**7-((4-((Benzyl(methylamino)methyl)benzyl)oxy)-4-(difluoro-** 940  
**methyl)-2H-chromen-2-one (19).** To a solution of **18** (0.27 mmol, 941  
0.11 g) in dry CH<sub>2</sub>Cl<sub>2</sub> (2 mL) at 0 °C under N<sub>2</sub> atmosphere was slowly 942  
dropped DAST (0.49 mmol, 0.064 mL) via a syringe. After 10 min, the 943  
reaction mixture was allowed to warm to room temperature and stirred 944  
overnight. The reaction mixture was then cooled to 0 °C with an 945  
external ice bath and carefully quenched with 10 mL of saturated aq. 946  
NaHCO<sub>3</sub>. The mixture was then extracted with dichloromethane (3 × 947  
15 mL). The collected organic layers were dried over anhydrous 948  
Na<sub>2</sub>SO<sub>4</sub> and concentrated under rotary evaporation. The crude 949  
residue was purified by column chromatography (eluent: ethyl acetate 950  
in CH<sub>2</sub>Cl<sub>2</sub>, 0.5%). Yield: 16%; colorless oil. <sup>1</sup>H NMR (500 MHz, 951  
CDCl<sub>3</sub>) δ: 7.61 (d, *J* = 8.9 Hz, 1H), 7.44–7.34 (m, 6H), 7.32 (t, *J* = 7.5 952  
Hz, 2H), 7.25–7.22 (m, 1H), 6.97 (dd, *J* = 8.9, 2.5 Hz, 1H), 6.94 (d, *J* = 953  
2.5 Hz, 1H), 6.70 (t, *J* = 53.8 Hz, 1H), 6.46 (s, 1H), 5.13 (s, 2H), 3.53 954  
(s, 4H), 2.19 (s, 3H). <sup>13</sup>C NMR (126 MHz, CDCl<sub>3</sub>) δ: 162.28 (s), 955  
160.00 (s), 156.14 (s), 145.13 (t, *J* = 22.3 Hz), 135.22–133.76 (m), 956  
129.51 (s), 129.48 (s), 129.09 (s), 128.34 (s), 127.59 (s), 127.55 (s), 957  
127.26 (s), 125.82 (t, *J* = 1.8 Hz), 113.67 (s), 112.14 (t, *J* = 242.4 Hz), 958  
111.80 (t, *J* = 8.8 Hz), 108.58 (s), 102.39 (s), 70.42 (s), 61.61 (s), 61.18 959  
(s), 41.98 (s). Anal. (C<sub>26</sub>H<sub>23</sub>F<sub>2</sub>NO<sub>3</sub>) calcd % C, 71.71; H, 5.32; N, 3.22; 960  
found % C, 71.55; H, 5.36; N, 3.21. HRMS (Q-TOF) calcd for 961  
(C<sub>26</sub>H<sub>23</sub>F<sub>2</sub>NO<sub>3</sub>): [M + H]<sup>+</sup> *m/z*: 436.1719, found 436.1728; [M + 962  
Na]<sup>+</sup> *m/z*: 458.1538, found 458.1547. 963

**4-(Hydroxymethyl)-7-((4-((3-hydroxypropyl)(methylamino)-** 964  
**methyl)benzyl)oxy)-2H-chromen-2-one (24).** Method E: prepared 965  
from **12a** (0.24 mmol, 0.076 g), 3-bromo-1-propanol (0.22 mmol, 20 966  
μL) and KI (cat.). Purification procedure: column chromatography 967  
(gradient eluent: methanol in CH<sub>2</sub>Cl<sub>2</sub>, 10%). Yield: 34%; glass solid. <sup>1</sup>H 968  
NMR (500 MHz, DMSO-*d*<sub>6</sub>) δ: 7.60 (d, *J* = 8.8 Hz, 1H), 7.39 (d, *J* = 8.0 969  
Hz, 2H), 7.29 (d, *J* = 8.0 Hz, 2H), 7.07 (d, *J* = 2.5 Hz, 1H), 6.99 (dd, *J* = 970  
8.8, 2.5 Hz, 1H), 6.28 (s, 1H), 5.61 (s, 1H, dis. with D<sub>2</sub>O), 5.18 (s, 2H), 971  
4.71 (s, 2H), 4.40 (s, 1H, dis. with D<sub>2</sub>O), 3.43 (s, 2H), 3.41 (t, *J* = 6.5 972  
Hz, 2H), 2.36 (t, *J* = 6.5 Hz, 2H), 2.07 (s, 3H), 1.59 (qn, *J* = 6.5 Hz, 973  
2H). <sup>13</sup>C NMR (126 MHz, DMSO-*d*<sub>6</sub>) δ: 161.69 (s), 160.89 (s), 974  
157.12 (s), 155.14 (s), 139.65 (s), 135.13 (s), 129.19 (s), 128.24 (s), 975  
125.85 (s), 113.12 (s), 111.27 (s), 107.94 (s), 102.19 (s), 70.19 (s), 976

977 61.75 (s), 59.84 (s), 59.53 (s), 54.62 (s), 42.28 (s), 30.63 (s). Anal.  
978 (C<sub>22</sub>H<sub>25</sub>NO<sub>3</sub>) calcd % C, 68.91; H, 6.57; N, 3.65; found % C, 69.07; H,  
979 6.50; N, 3.54. HRMS (Q-TOF) calcd for (C<sub>22</sub>H<sub>25</sub>NO<sub>3</sub>): [M - H]<sup>-</sup> m/  
980 z: 382.1660, found 382.1652; [M + Na]<sup>+</sup> m/z: 406.1625, found  
981 406.1630.

982 **Enzyme Inhibition Studies.** All enzymes and reagents were from  
983 Sigma-Aldrich Italy. Experiments were performed in 96-well plate-  
984 based assays using a multiplate reader Infinite M1000 Pro (Tecan,  
985 Cernusco sul Naviglio, Italy) and were run in triplicate. The 96-well  
986 plates were purchased from Greiner Bio-One (Kremsmenster, Austria).  
987 IC<sub>50</sub> values were obtained by nonlinear regression using Prism software  
988 (GraphPad Prism version 5.00 for Windows, GraphPad Software, San  
989 Diego, CA). Inhibition of human recombinant AChE and horse serum  
990 BChE was determined by applying already published procedures<sup>43</sup>  
991 based on Ellman's spectrophotometric assay,<sup>42</sup> using transparent, flat-  
992 bottom plates. For human recombinant MAO A/B inhibition studies,  
993 the spectrofluorimetric protocol, based on the oxidative deamination of  
994 kynuramine to 4-hydroxyquinoline,<sup>33</sup> was performed in black, flat-  
995 bottom plates. The same protocol was adopted for the spectrophoto-  
996 metric detection of 4-hydroxyquinoline (absorbance at 316 nm) in  
997 transparent, flat-bottom plates as previously described.<sup>18</sup>

## 998 ■ ASSOCIATED CONTENT

### 999 51 Supporting Information

1000 The Supporting Information is available free of charge at  
1001 <https://pubs.acs.org/doi/10.1021/acs.jmedchem.1c01784>.

1002 Protocols for early-ADME experiments (kinetic solubility,  
1003 PAMPA-HDM, PAMPA-BBB, log *D*<sub>7.4p</sub> CHI, HSA bind-  
1004 ing, Caco-2 permeability, microsomal stability, and  
1005 cytochrome P450 3A4 inhibition); absorbance protocol  
1006 for MAO B inhibition; reversibility MAO B binding  
1007 assays; and methods for molecular docking simulations  
1008 (PDF)

1009 Molecular formula strings (MFS) (CSV)

1010 Docking complexes (compound 15 docked with hAChE  
1011 and hMAO B) (PDB)

1012 Cell-based assay protocols (SH-SY5Y and HepG2  
1013 cytotoxicity, neuroprotection) (PDF)

1014 2v5z\_full\_validation (PDF)

1015 4ey7\_full\_validation (PDF)

## 1016 ■ AUTHOR INFORMATION

### 1017 Corresponding Author

1018 **Leonardo Pisani** – Department of Pharmacy—Pharmaceutical  
1019 Sciences, University of Bari “Aldo Moro”, 70125 Bari, Italy;  
1020 [orcid.org/0000-0002-4198-3897](https://orcid.org/0000-0002-4198-3897); Phone: +39-  
1021 0805442803; Email: [leonardo.pisani@uniba.it](mailto:leonardo.pisani@uniba.it); Fax: +39-  
1022 080-5442230

### 1023 Authors

1024 **Mariagrazia Rullo** – Department of Pharmacy—  
1025 Pharmaceutical Sciences, University of Bari “Aldo Moro”,  
1026 70125 Bari, Italy; [orcid.org/0000-0001-5304-6764](https://orcid.org/0000-0001-5304-6764)

1027 **Marco Cipolloni** – TES Pharma s.r.l., 06121 Perugia, Italy

1028 **Marco Catto** – Department of Pharmacy—Pharmaceutical  
1029 Sciences, University of Bari “Aldo Moro”, 70125 Bari, Italy;  
1030 [orcid.org/0000-0002-8411-304X](https://orcid.org/0000-0002-8411-304X)

1031 **Carolina Colliva** – TES Pharma s.r.l., 06121 Perugia, Italy;  
1032 [orcid.org/0000-0002-1675-3141](https://orcid.org/0000-0002-1675-3141)

1033 **Daniela Valeria Miniero** – Department of Biosciences,  
1034 Biotechnologies and Biopharmaceutics, University of Bari  
1035 “Aldo Moro”, 70125 Bari, Italy; [orcid.org/0000-0002-3324-9692](https://orcid.org/0000-0002-3324-9692)  
1036

**Tiziana Latronico** – Department of Biosciences, Biotechnologies  
and Biopharmaceutics, University of Bari “Aldo Moro”, 70125  
Bari, Italy; [orcid.org/0000-0001-6971-5416](https://orcid.org/0000-0001-6971-5416)

**Modesto de Candia** – Department of Pharmacy—  
Pharmaceutical Sciences, University of Bari “Aldo Moro”,  
70125 Bari, Italy

**Tiziana Benicchi** – TES Pharma s.r.l., 06121 Perugia, Italy

**Anna Linusson** – Department of Chemistry, Umeå University,  
90187 Umeå, Sweden; [orcid.org/0000-0003-0063-8912](https://orcid.org/0000-0003-0063-8912)

**Nicola Giacchè** – TES Pharma s.r.l., 06121 Perugia, Italy;  
[orcid.org/0000-0002-4810-3960](https://orcid.org/0000-0002-4810-3960)

**Cosimo Damiano Altomare** – Department of Pharmacy—  
Pharmaceutical Sciences, University of Bari “Aldo Moro”,  
70125 Bari, Italy

Complete contact information is available at:  
<https://pubs.acs.org/doi/10.1021/acs.jmedchem.1c01784>

## Notes

The authors declare no competing financial interest.

## ■ ABBREVIATIONS USED

AChE, acetylcholinesterase; AD, Alzheimer's disease; BBB,  
blood–brain barrier; BChE, butyrylcholinesterase; CAS, cata-  
lytic anionic subsite; CNS, central nervous system; CHI,  
chromatographic hydrophobicity index; CL<sub>int</sub>, intrinsic clear-  
ance; DAST, (diethylamino)sulfur trifluoride; DMAP, 4-  
(dimethylamino)pyridine; ER, efflux ratio; HDM, hexadecane  
membrane; HSA, human serum albumin; MAO, monoamine  
oxidase; MTT, 3-(4,5-dimethylthiazol-2-yl)-2,5-diphenyl-tetra-  
zolium bromide; ND, neurodegenerative disease; NMDA, N-  
methyl-D-aspartate; *P*<sub>app</sub>, apparent permeability; PAMPA,  
parallel artificial membrane permeability assay; PAS, peripheral  
anionic subsite; PBLE, porcine brain lipid extracts; PBS,  
phosphate-buffered saline; PCC, pyridinium chlorochromate;  
P-gp, P-glycoprotein; Q-TOF, Quadrupole Time-of-Flight;  
ROS, reactive oxygen species; RP-HPLC, reversed-phase high-  
performance liquid chromatography; SAR, structure–activity  
relationships; SPR, surface plasmon resonance; TEER, trans-  
epithelial electrical resistance; TLC, thin-layer chromatography

## ■ REFERENCES

- (1) 2020 Alzheimer's Disease Facts and Figures. *Alzheimer's Dementia* 2020, 16 (3), 391–460.
- (2) Saez-Atienzar, S.; Masliah, E. Cellular Senescence and Alzheimer Disease: The Egg and the Chicken Scenario. *Nat. Rev. Neurosci.* 2020, 21, 433–444.
- (3) Dubois, B.; Feldman, H. H.; Jacova, C.; Cummings, J. L.; DeKosky, S. T.; Barberger-Gateau, P.; Delacourte, A.; Frisoni, G.; Fox, N. C.; Galasko, D.; Gauthier, S.; Hampel, H.; Jicha, G. A.; Meguro, K.; Pasquier, F.; Robert, P.; Rossor, M.; Salloway, S.; Sarazin, M.; de Souza, L. C.; Stern, Y.; Visser, P. J.; Scheltens, P.; O'Brien, J. Position Paper Revising the Defi Nition of Alzheimer's Disease: A New Lexicon. *Lancet Neurol.* 2010, 9, 1118–1127.
- (4) Querfurth, H. W.; LaFerla, F. M. Alzheimer's Disease: Mechanism of Disease. *N. Engl. J. Med.* 2010, 362, 329–344.
- (5) Domingo-Fernández, D.; Kodamullil, A. T.; Iyappan, A.; Naz, M.; Emon, M. A.; Raschka, T.; Karki, R.; Springstube, S.; Ebeling, C.; Hofmann-Apitius, M. Multimodal Mechanistic Signatures for Neurodegenerative Diseases (NeuroMMSig): A Web Server for Mechanism Enrichment. *Bioinformatics* 2017, 33, 3679–3681.
- (6) Citron, M. Alzheimer's Disease: Strategies for Disease Modification. *Nat. Rev. Drug Discovery* 2010, 9, 387–398.

- (7) Wang, H.; Zhang, H. Reconsideration of Anticholinesterase Therapeutic Strategies against Alzheimer's Disease. *ACS Chem. Neurosci.* **2019**, *10*, 852–862.
- (8) Mangialasche, F.; Solomon, A.; Winblad, B.; Mecocci, P.; Kivipelto, M. Alzheimer's Disease: Clinical Trials and Drug Development. *Lancet. Neurol.* **2010**, *9*, 702–716.
- (9) Cummings, J. L.; Morstorf, T.; Zhong, K. Alzheimer's Disease Drug-Development Pipeline: Few Candidates, Frequent Failures. *Alzheimer's Res. Ther.* **2014**, *6*, No. 37.
- (10) Cummings, J.; Lee, G.; Ritter, A.; Sabbagh, M.; Zhong, K. Alzheimer's Disease Drug Development Pipeline: 2020. In *Alzheimer's & Dementia: Translational Research & Clinical Interventions*; Wiley Online Library, 2020; Vol. 6.
- (11) León, R.; Garcia, A. G.; Marco-Contelles, J. Recent Advances in the Multitarget-Directed Ligands Approach for the Treatment of Alzheimer's Disease. *Med. Res. Rev.* **2013**, *33*, 139–189.
- (12) Lecoutey, C.; Hedou, D.; Freret, T.; Giannoni, P.; Gaven, F.; Since, M.; Bouet, V.; Ballandonne, C.; Corvaisier, S.; Malzert Freon, A.; Mignani, S.; Cresteil, T.; Boulouard, M.; Claeysen, S.; Rochais, C.; Dallemagne, P. Design of Donecopride, a Dual Serotonin Subtype 4 Receptor Agonist/Acetylcholinesterase Inhibitor with Potential Interest for Alzheimer's Disease Treatment. *Proc. Natl. Acad. Sci. U.S.A.* **2014**, *111*, E3825–E3830.
- (13) Malek, R.; Arribas, R. L.; Palomino-Antolin, A.; Totoston, P.; Demougeot, C.; Kobrlova, T.; Soukup, O.; Iriepa, I.; Moraleda, I.; Diez-Iriepa, D.; Godyń, J.; Panek, D.; Malawska, B.; Gluch-Lutwin, M.; Mordyl, B.; Siwek, A.; Chabchoub, F.; Marco-Contelles, J.; Kiec-Kononowicz, K.; Egea, J.; de los Ríos, C.; Ismaili, L. New Dual Small Molecules for Alzheimer's Disease Therapy Combining Histamine H<sub>3</sub> Receptor (H<sub>3</sub>R) Antagonism and Calcium Channels Blockade with 1126 Additional Cholinesterase Inhibition. *J. Med. Chem.* **2019**, *62*, 11416–11422.
- (14) Oukoloff, K.; Coquelle, N.; Bartolini, M.; Naldi, M.; Le Guevel, R.; Bach, S.; Josselin, B.; Ruchaud, S.; Catto, M.; Pisani, L.; Denora, N.; Iacobazzi, R. M.; Silman, I.; Sussman, J. L.; Buron, F.; Colletier, J.-P.; Jean, L.; Routier, S.; Renard, P.-Y. Design, Biological Evaluation and X-Ray Crystallography of Nanomolar Multifunctional Ligands Targeting 1133 Simultaneously Acetylcholinesterase and Glycogen Synthase Kinase-3. *Eur. J. Med. Chem.* **2019**, *168*, 58–77.
- (15) Simoni, E.; Daniele, S.; Bottegoni, G.; Pizzirani, D.; Trincavelli, M. L.; Goldoni, L.; Tarozzo, G.; Reggiani, A.; Martini, C.; Piomelli, D.; Melchiorre, C.; Rosini, M.; Cavalli, A. Combining Galantamine and 1138 Memantine in Multitargeted, New Chemical Entities Potentially Useful 1139 in Alzheimer's Disease. *J. Med. Chem.* **2012**, *55*, 9708–9721.
- (16) Brunschweiler, A.; Koch, P.; Schlenk, M.; Pineda, F.; Küppers, P.; Hinz, S.; Köse, M.; Ullrich, S.; Hockemeyer, J.; Wiese, M.; Heer, J.; Müller, C. E. 8-Benzyltetrahydropyrazino[2,1-f]Purinediones: Water- 1143 Soluble Tricyclic Xanthine Derivatives as Multitarget Drugs for 1144 Neurodegenerative Diseases. *ChemMedChem* **2014**, *53*, 1704–1724.
- (17) Bautista-Aguilera, s. M.; Hagenow, S.; Palomino-Antolin, A.; 1146 Farré-Alins, V.; Ismaili, L.; Joffrin, P.-L.; Jimeno, M. L.; Soukup, O.; 1147 Janočková, J.; Kalinowsky, L.; Proschak, E.; Iriepa, I.; Moraleda, I.; 1148 Schwed, J. S.; Romero Martínez, A.; López-Muñoz, F.; Chioua, M.; 1149 Egea, J.; Ramsay, R. R.; Marco-Contelles, J.; Stark, H. Multitarget- 1150 Directed Ligands Combining Cholinesterase and Monoamine Oxidase 1151 Inhibition with Histamine H<sub>3</sub> R Antagonism for Neurodegenerative 1152 Diseases. *Angew. Chem., Int. Ed.* **2017**, *56*, 12765–12769.
- (18) Pisani, L.; Iacobazzi, R. M.; Catto, M.; Rullo, M.; Farina, R.; 1154 Denora, N.; Cellamare, S.; Altomare, C. D. Investigating Alkyl Nitrates 1155 as Nitric Oxide Releasing Precursors of Multitarget Acetylcholinester- 1156 ase-Monoamine Oxidase B Inhibitors. *Eur. J. Med. Chem.* **2019**, *161*, 1157 292–309.
- (19) Rullo, M.; Catto, M.; Carrieri, A.; de Candia, M.; Altomare, C. 1159 D.; Pisani, L. Chasing ChEs-MAO B Multi-Targeting 4-Aminomethyl- 1160 7-Benzoyloxy-2H-Chromen-2-Ones. *Molecules* **2019**, *24*, No. 4507.
- (20) Košak, U.; Strašek, N.; Knez, D.; Jukič, M.; Žakelj, S.; Zahirović, 1162 A.; Pišlar, A.; Brazzolotto, X.; Nachon, F.; Kos, J.; Gobec, S. N- 1163 Alkylpiperidine Carbamates as Potential Anti-Alzheimer's Agents. *Eur.* 1164 *J. Med. Chem.* **2020**, *197*, No. 112282.
- (21) He, Q.; Liu, J.; Lan, J.-S.; Ding, J.; Sun, Y.; Fang, Y.; Jiang, N.; 1165 Yang, Z.; Sun, L.; Jin, Y.; Xie, S.-S. Coumarin-Dithiocarbamate Hybrids 1166 as Novel Multitarget AChE and MAO-B Inhibitors against Alzheimer's 1167 Disease: Design, Synthesis and Biological Evaluation. *Bioorg. Chem.* 1168 **2018**, *81*, 512–528.
- (22) Reis, J.; Cagide, F.; Valencia, M. E.; Teixeira, J.; Bagetta, D.; 1170 Pérez, C.; Uriarte, E.; Oliveira, P. J.; Ortuso, F.; Alcaro, S.; Rodríguez- 1171 Franco, M. I.; Borges, F. Multi-Target-Directed Ligands for Alzheimer's 1172 Disease: Discovery of Chromone-Based Monoamine Oxidase/ 1173 Cholinesterase Inhibitors. *Eur. J. Med. Chem.* **2018**, *158*, 781–800.
- (23) Kumar, B.; Dwivedi, A. R.; Sarkar, B.; Gupta, S. K.; 1175 Krishnamurthy, S.; Mantha, A. K.; Parkash, J.; Kumar, V. 4,6- 1176 Diphenylpyrimidine Derivatives as Dual Inhibitors of Monoamine 1177 Oxidase and Acetylcholinesterase for the Treatment of Alzheimer's 1178 Disease. *ACS Chem. Neurosci.* **2019**, *10*, 252–265.
- (24) Xu, Y.; Zhang, H.; Wang, H.; Mao, F.; Bao, K.; Liu, W.; Zhu, J.; Li, 1180 X.; Zhang, H.; Li, J. Rational Design of Novel Selective Dual-Target 1181 Inhibitors of Acetylcholinesterase and Monoamine Oxidase B as 1182 Potential Anti-Alzheimer's Disease Agents. *ACS Chem. Neurosci.* **2019**, 1183 *10*, 482–496.
- (25) Inestrosa, N. C.; Dinamarca, M. C.; Alvarez, A. Amyloid- 1185 Cholinesterase Interactions. Implications for Alzheimer's Disease. 1186 *FEBS J.* **2008**, *275*, 625–632.
- (26) Kim, D.; Hoon Baik, S.; Kang, S.; Won Cho, S.; Bae, J.; Cha, M.- 1188 Y.; J Sailor, M.; Mook-Jung, I.; Han Ahn, K. Close Correlation of 1189 Monoamine Oxidase Activity with Progress of Alzheimer's Disease in 1190 Mice, Observed by in Vivo Two-Photon Imaging. *ACS Cent. Sci.* **2016**, 1191 *2*, 967–975.
- (27) Gulyás, B.; Pavlova, E.; Kása, P.; Gulya, K.; Bakota, L.; Várszegi, 1193 S.; Keller, E.; Horváth, M. C.; Nag, S.; Hermeicz, I.; Magyar, K.; Halldin, 1194 C. Activated MAO-B in the Brain of Alzheimer Patients, Demonstrated 1195 by [<sup>11</sup>C]-L-Deprenyl Using Whole Hemisphere Autoradiography. 1196 *Neurochem. Int.* **2011**, *58*, 60–68.
- (28) Saura, J.; Luque, J. M.; Cesura, A. M.; Prada, M. Da.; Chan-Palay, 1198 V.; Huber, G.; Löffler, J.; Richards, J. G. Increased Monoamine Oxidase 1199 b Activity in Plaque-Associated Astrocytes of Alzheimer Brains 1200 Revealed by Quantitative Enzyme Radioautography. *Neuroscience* 1201 **1994**, *62*, 15–30.
- (29) Weinreb, O.; Amit, T.; Bar-Am, O.; Youdim, M. B. H. Ladostigil: 1203 A Novel Multimodal Neuroprotective Drug with Cholinesterase and 1204 Brain-Selective Monoamine Oxidase Inhibitory Activities for Alz- 1205 heimer's Disease Treatment. *Curr. Drug Targets* **2012**, *13*, 483–494.
- (30) Schneider, L. S.; Geffen, Y.; Rabinowitz, J.; Thomas, R. G.; 1207 Schmidt, R.; Ropele, S.; Weinstock, M. Ladostigil Study Group. Low- 1208 Dose Ladostigil for Mild Cognitive Impairment: A Phase 2 Placebo- 1209 Controlled Clinical Trial. *Neurology* **2019**, *93*, e1474–e1484.
- (31) Al-Warhi, T.; Sabt, A.; Elkaeed, E. B.; Eldehna, W. M. Recent 1211 Advancements of Coumarin-Based Anticancer Agents: An up-to-Date 1212 Review. *Bioorg. Chem.* **2020**, *103*, No. 104163.
- (32) Bhagat, K.; Bhagat, J.; Gupta, M. K.; Singh, J. V.; Gulati, H. K.; 1214 Singh, A.; Kaur, K.; Kaur, G.; Sharma, S.; Rana, A.; Singh, H.; Sharma, 1215 S.; Singh Bedi, P. M. Design, Synthesis, Antimicrobial Evaluation, and 1216 Molecular Modeling Studies of Novel Indolinedione–Coumarin 1217 Molecular Hybrids. *ACS Omega* **2019**, *4*, 8720–8730.
- (33) Pisani, L.; Farina, R.; Catto, M.; Iacobazzi, R. M.; Nicolotti, O.; 1219 Cellamare, S.; Mangiatordi, G. F.; Denora, N.; Soto-Otero, R. R.; 1220 Siragusa, L.; Altomare, C. D.; Carotti, A. Exploring Basic Tail 1221 Modifications of Coumarin-Based Dual Acetylcholinesterase-Mono- 1222 amine Oxidase B Inhibitors: Identification of Water-Soluble, Brain- 1223 Permeant Neuroprotective Multitarget Agents. *J. Med. Chem.* **2016**, *59*, 1224 6791–6806.
- (34) Farina, R.; Pisani, L.; Catto, M.; Nicolotti, O.; Gadaleta, D.; 1226 Denora, N.; Soto-Otero, R.; Mendez-Alvarez, E.; Passos, C. S.; 1227 Muncipinto, G.; Altomare, C. D.; Nurisso, A.; Carrupt, P.-A.; Carotti, 1228 A. Structure-Based Design and Optimization of Multitarget-Directed 2 1229 H -Chromen-2-One Derivatives as Potent Inhibitors of Monoamine 1230 Oxidase B and Cholinesterases. *J. Med. Chem.* **2015**, *58*, 5561–5578.
- (35) Haggmann, W. K. The Many Roles for Fluorine in Medicinal 1232 Chemistry. *J. Med. Chem.* **2008**, *51*, 4359–4369. 1233

- 1234 (36) Böhm, H.; Banner, D.; Bendels, S.; Kansy, M.; Kuhn, B.; Müller,  
1235 K.; Obst-Sander, U.; Stahl, M. Fluorine in Medicinal Chemistry.  
1236 *ChemBioChem* **2004**, *5*, 637–643.
- 1237 (37) Meanwell, N. A. Fluorine and Fluorinated Motifs in the Design  
1238 and Application of Bioisosters for Drug Design. *J. Med. Chem.* **2018**,  
1239 *61*, 5822–5880.
- 1240 (38) Gillis, E. P.; Eastman, K. J.; Hill, M. D.; Donnelly, D. J.;  
1241 Meanwell, N. A. Applications of Fluorine in Medicinal Chemistry. *J.*  
1242 *Med. Chem.* **2015**, *58*, 8315–8359.
- 1243 (39) Zafrani, Y.; Sod-Moriah, G.; Yeffet, D.; Berliner, A.; Amir, D.;  
1244 Marciano, D.; Elias, S.; Katalan, S.; Ashkenazi, N.; Madmon, M.;  
1245 Gershonov, E.; Saphier, S. CF<sub>2</sub>H, a Functional Group-Dependent  
1246 Hydrogen-Bond Donor: Is It a More or Less Lipophilic Bioisostere of  
1247 OH, SH, and CH<sub>3</sub>? *J. Med. Chem.* **2019**, *62*, 5628–5637.
- 1248 (40) Zafrani, Y.; Yeffet, D.; Sod-Moriah, G.; Berliner, A.; Amir, D.;  
1249 Marciano, D.; Gershonov, E.; Saphier, S. Difluoromethyl Bioisostere:  
1250 Examining the “Lipophilic Hydrogen Bond Donor” Concept. *J. Med.*  
1251 *Chem.* **2017**, *60*, 797–804.
- 1252 (41) Vorberg, R.; Trapp, N.; Zimmerli, D.; Wagner, B.; Fischer, H.;  
1253 Kratochwil, N. A.; Kansy, M.; Carreira, E. M.; Müller, K. Effect of  
1254 Partially Fluorinated N-Alkyl-Substituted Piperidine-2-Carboxamides  
1255 on Pharmacologically Relevant Properties. *ChemMedChem* **2016**, *11*,  
1256 2216–2239.
- 1257 (42) Ellman, G. L.; Courtney, K. D.; Andres, V.; Featherstone, R. M. A  
1258 New and Rapid Colorimetric Determination of Acetylcholinesterase  
1259 Activity. *Biochem. Pharmacol.* **1961**, *7*, 88–90.
- 1260 (43) Pisani, L.; Catto, M.; De Palma, A.; Farina, R.; Cellamare, S.;  
1261 Altomare, C. D. Discovery of Potent Dual Binding Site Acetylcholi-  
1262 nesterase Inhibitors via Homo- and Heterodimerization of Coumarin-  
1263 Based Moieties. *ChemMedChem* **2017**, *12*, 1349–1358.
- 1264 (44) Blackwell, B.; Mabbitt, L. A. Tyramine in Cheese Related to  
1265 Hypertensive Crises After Monoamine-Oxidase Inhibition. *Lancet*  
1266 **1965**, *285*, 938–940.
- 1267 (45) Purgatorio, R.; de Candia, M.; Catto, M.; Carrieri, A.; Pisani, L.;  
1268 De Palma, A.; Toma, M.; Ivanova, O. A. O. A.; Voskressensky, L. G. L.  
1269 G.; Altomare, C. D. C. D. Investigating 1,2,3,4,5,6-Hexahydroazepino-  
1270 [4,3-b]Indole as Scaffold of Butyrylcholinesterase-Selective Inhibitors  
1271 with Additional Neuroprotective Activities for Alzheimer’s Disease.  
1272 *Eur. J. Med. Chem.* **2019**, *177*, 414–424.
- 1273 (46) Sterling, T.; Irwin, J. J. ZINC 15 – Ligand Discovery for  
1274 Everyone. *J. Chem. Inf. Model.* **2015**, *55*, 2324–2337.
- 1275 (47) Baell, J. B.; Holloway, G. A. New Substructure Filters for  
1276 Removal of Pan Assay Interference Compounds (PAINS) from  
1277 Screening Libraries and for Their Exclusion in Bioassays. *J. Med.*  
1278 *Chem.* **2010**, *53*, 2719–2740.
- 1279 (48) Lagorce, D.; Sperandio, O.; Baell, J. B.; Miteva, M. A.; Villoutreix,  
1280 B. O. FAF-Drugs3: A Web Server for Compound Property Calculation  
1281 and Chemical Library Design. *Nucleic Acids Res.* **2015**, *43*, W200–  
1282 W207.
- 1283 (49) Aldrich, C.; Bertozzi, C.; Georg, G. I.; Kiessling, L.; Lindsley, C.;  
1284 Liotta, D.; Merz, K. M.; Schepartz, A.; Wang, S. The Ecstasy and Agony  
1285 of Assay Interference Compounds. *J. Med. Chem.* **2017**, *60*, 2165–2168.
- 1286 (50) Valkó, K.; Bevan, C.; Reynolds, D. Chromatographic Hydro-  
1287 phobicity Index by Fast-Gradient RP-HPLC: A High-Throughput  
1288 Alternative to Log P/Log D. *Anal. Chem.* **1997**, *69*, 2022–2029.
- 1289 (51) Wager, T. T.; Chandrasekaran, R. Y.; Hou, X.; Troutman, M. D.;  
1290 Verhoest, P. R.; Villalobos, A.; Will, Y. Defining Desirable Central  
1291 Nervous System Drug Space through the Alignment of Molecular  
1292 Properties, in Vitro ADME, and Safety Attributes. *ACS Chem. Neurosci.*  
1293 **2010**, *1*, 420–434.
- 1294 (52) Purgatorio, R.; Candia, M.; Catto, M.; Rullo, M.; Pisani, L.;  
1295 Denora, N.; Carrieri, A.; Nevskaya, A. A.; Voskressensky, L. G.;  
1296 Altomare, C. D. Evaluation of Water-Soluble Mannich Base Prodrugs of  
1297 2,3,4,5-Tetrahydroazepino[4,3-b]Indol-1(6H)-one as Multitarget-  
1298 Directed Agents for Alzheimer’s Disease. *ChemMedChem* **2021**, *16*,  
1299 589–598.
- 1300 (53) Rich, R. L.; Day, Y. S. N.; Morton, T. A.; Myszka, D. G. High-  
1301 Resolution and High-Throughput Protocols for Measuring Drug/  
Human Serum Albumin Interactions Using BIACORE. *Anal. Biochem.* **2001**, *296*, 197–207.
- (54) Frostell-Karlsson, Å.; Remaeus, A.; Roos, H.; Andersson, K.;  
Borg, P.; Hämäläinen, M.; Karlsson, R. Biosensor Analysis of the  
Interaction between Immobilized Human Serum Albumin and Drug  
Compounds for Prediction of Human Serum Albumin Binding Levels.  
*J. Med. Chem.* **2000**, *43*, 1986–1992.
- (55) Pisani, L.; Catto, M.; Giangreco, I.; Leonetti, F.; Nicolotti, O.;  
Stefanachi, A.; Cellamare, S.; Carotti, A. Design, Synthesis, and  
Biological Evaluation of Coumarin Derivatives Tethered to an  
Edrophonium-like Fragment as Highly Potent and Selective Dual  
Binding Site Acetylcholinesterase Inhibitors. *ChemMedChem* **2010**, *5*,  
1616–1630.
- (56) Pisani, L.; Rullo, M.; Catto, M.; de Candia, M.; Carrieri, A.;  
Cellamare, S.; Altomare, C. D. Structure-Property Relationship Study  
of the HPLC Enantioselective Retention of Neuroprotective 7-[(1-  
Alkylpiperidin-3-yl)methoxy]Coumarin Derivatives on an Amylose-  
Based Chiral Stationary Phase. *J. Sep. Sci.* **2018**, *41*, 1376–1384.
- (57) Rullo, M.; Niso, M.; Pisani, L.; Carrieri, A.; Colabufo, N. A.;  
Cellamare, S.; Altomare, C. D. 1,2,3,4-Tetrahydroisquinoline/2H-  
Chromen-2-One Conjugates as Nanomolar P-Glycoprotein Inhibitors:  
Molecular Determinants for Affinity and Selectivity over Multidrug  
Resistance Associated Protein 1. *Eur. J. Med. Chem.* **2019**, *161*, 433–  
444.